Design, Fabrication, and Testing of a Dielectric Elastomer based Ambulatory Active Compression Device

by

Hamza Edher

A thesis
presented to the University of Waterloo
in fulfillment of the
thesis requirement for the degree of
Masters of Applied Science
in
Mechanical Engineering

Waterloo, Ontario, Canada, 2016

AUTHOR'S DECLARATION

I hereby declare that I am the sole author of this thesis. This is a true copy of the thesis, including any required final revisions, as accepted by my examiners.

I understand that my thesis may be made electronically available to the public.

Abstract

Various vascular disorders such as deep vein thrombosis and edema have been associated with the pooling of venous blood in the lower limbs due to extended periods of immobility. Prophylaxis against peripheral vascular diseases in the lower limbs commonly involves the utilization of external compression, in particular pneumatic active compression (PAC). Although effective, PAC systems require the use of an air compressor and flow system, and are therefore unsuitable for ambulatory use. In this research, a novel design for a dielectric elastomer (DE) based active compression device design is presented, fabricated, and experimentally validated.

The system comprises of a belt mechanism connected in conjunction with a DE actuator. The belt mechanism is utilized in order to overcome an intrinsic shortcoming of DE actuators and in turn allow active compression to be applied directly with voltage application. In doing so, the presented design reduces the period during which the actuator is charged thus improving system lifetime and power efficiency. Analytical models characterizing the operation of the belt mechanisms are formulated and validated experimentally with less than 7% error.

Both static and dynamic testing is conducted in order to characterize the effectiveness of the active compression device. It is determined that the actuation output amplitudes are reduced when actuating cyclically. To combat this, a novel method of dynamically charging DE actuators through manipulating the input signal shape, termed the hold method, is introduced. It is shown that through implementing the hold time method cyclic actuation output can be increased by 24% with insignificant change in the desired actuation output curve shape. The optimized hold time parameters obtained through cyclic DE force and strain testing are utilized for active compression testing and a physiologically beneficial pressure gradient of 10 mmHg is achieved.

A regenerative powering circuit and control system utilized to charge two capacitive elements sequentially by transferring charge from one component to the other is introduced. This circuit aims to increase the energy efficiency of the system and provides potential to be utilized in an active compression system where more than one active element is present. Preliminary testing is conducted on the circuit and the associated timing control system and it is shown to operate effectively for capacitive elements with low resistances, reducing the energy requirements to charge the second component by up to 25%.

Acknowledgements

First, my sincere appreciation goes to my supervisor, Prof. Armaghan Salehian. Your continued guidance and constructive feedback was fundamental to the success of this research. I would also like to thank Dr. Keyma Prince and Prof. Sean Peterson for their involvement and valuable suggestions.

Prof. Iain Anderson and Ben Pocock, thank for hoisting me on your shoulders and helping immerse me in the world of dielectric elastomers. The experience and knowledge gained during my time at the Biomimetics Lab in Auckland has been invaluable throughout the course of this research.

To all my lab mates, I thank you for making my time at the lab more enjoyable, and for all your support and valuable comments over the course of my time here. Blake, thank you for making sure that we got our share of Vitamin D (aka sunlight) every morning. Egon, for helping motivate me to achieve my potential in the lab and in the gym. A special thanks to Steven Lao, who was an integral part of this research. Louise, you were there in the very beginning when this was all just a drawing on a piece a paper, the countless hours spent brainstorming and molding mannequin legs were integral to the completion of this work.

I cannot begin to express my immense gratitude to my family for helping shape the man I am today and for their loving support throughout my entire life. Everything good in me, I owe to you. To my friends, thank you all for making sure this experience was as enjoyable as it was rewarding. The not-so-good in me, I attribute to you.

Finally, I express my appreciation to Lockheed Martin for funding this research.

Dedication

This work is dedicated to my parents and my two brothers, Faraj and Ziyad.

Table of Contents

List of Figures

List of Tables

Nomenclature

Variable/parameter	Symbol	Units
Capacitance	C	F
Dielectric permittivity - relative	ε_r	-
Dielectric permittivity - vacuum	ε_o	F m^{-1}
Electric field	E	V m^{-1}
Energy stored in a capacitor	E_{cap}	J
Force: applied by the spring	F_{sp}	N
Force: electrical (force exerted by actuator due to electrical loading)	F_e	N
Force: mech (force exerted by actuator due to mechanical loading)	F_m	N
Force: tangential (applied on the ends of belt mechanism)	F_t	N
Force: tensional (applied by the DE actuator)	F_{DE}	N
Length of actuator: initial	l_{1o}	m
Length of actuator: after pre-stretch	l_1	m
Pressure applied on test bed: radial	P	Pa
Pressure: Actuation (Maxwell stress)	p	Pa
Pressure change with actuator activation	ΔP	Pa
Radius of cylindrical test bed	r	m
Spring constant	k	N m^{-1}
Spring length: compressed	L_s	m
Spring length: uncompressed	L_{os}	m
Spring rate constant	c	N
Stress: mech (stress exerted by actuator due to mechanical loading)	T_m	Pa
Stretch ratio: mechanical	λ_{mi}	-
Thickness of dielectric layer: After pre-stretch	d	m
Thickness of dielectric layer: Initial	d_o	m
Time: Hold time	t_h	ms
Time: Rise time	t_r	ms
Time: Total pulse duration	t_f	ms

Voltage	V	V
Voltage – Dynamic (two term Fourier Series fit)	$V(t)$	V
Voltage – Dynamic (maximum amplitude)	V_{max}	V
Width of actuator: After pre-stretch	W	m
Width of actuator: Initial	W_o	m
Width of belt mechanism	w	m
Young's modulus	Y	Pa

Chapter 1
Introduction – The Second Heart

The cardiovascular system, powered by the heart, is responsible for the transport of blood through the arteries to the body's organs and muscles. This blood provides oxygen, nutrients, hormones, and other important substances to the body to provide energy, fight diseases, and maintain homeostasis [1]. While the heart is very effective in pushing the blood through the arteries in the body, returning the blood back to the heart through the veins requires the aid of the "Second Heart". The calf muscles, aka soleus, work as a "Second Heart" through aiding in the return of blood from the lower extremities to the heart and in turn promoting blood circulation and reducing venous pooling [2]. Blood pooling due to the stasis of venous blood in the lower extremities has been associated with various disorders such as Deep Vein Thrombosis (DVT), reduced blood flow, and edema [3]. This pooling of venous blood can be attributed in part to substantial periods of immobility in which the calf muscles are not contracting [4]. Furthermore, the insufficient pumping of the calf muscles inherent with these periods of immobility has been directly correlated with the development of a DVT [5]. Additional possible symptoms of reduced blood flow include swelling of the lower extremities, varicose veins, and ulcerations [5, 6].

A common prophylaxis for several vascular diseases including edema and DVT utilizes external compression solutions [7, 8]. Passive external compression utilizes graduated compression stockings to reduce venous caliper and augment venous return. The efficacy of this method is commonly challenged due to the passive nature of the compression, where the load applied by the compression sock is constant throughout the cardiac cycle and can vary across more than one application. Active compression in the form of intermittent pneumatic compression was found to be significantly more beneficial in improving physiological hemodynamic responses [9, 10]. This is commonly achieved through utilizing several air cuffs which are attached in series from the ankle to the knee and inflated sequentially. The subsequent applied "milking" pressure promotes blood return from the lower extremities. As shown in Lao [11], a controllable air compressor allows for a robust design through changing the applied pressure and inflation-deflation times. Additionally, several studies suggest that active compression may also be beneficial for healthy individuals, where its effects on athlete performance, blood flow, recovery times, muscle oxygenation, and fatigue are examined in [12-15].

This work aims to provide an alternative to pneumatic external active compression systems which exhibit a major flaw. Although these systems have been found to incur positive physiological effects in the clinical setting, their intrinsic need for an air compressor and valve system restricts their use in an ambulatory setting. Therefore, there exists a need for an active compression system capable of operating in mobile scenarios. In order to achieve ambulatory active compression, a smart material solution is presented. Smart materials exhibit direct electro-mechanical coupling and in turn eliminate the need for an air compressor. Existing smart material active compression solutions fall short in several categories including achievable pressures, power efficiency, and some are temperature dependent. Additionally, existing work on smart material solutions is only presented for active compression applied statically.

In order to incur positive physiological effects, a pressure gradient of 10 mmHg must be achieved in cyclic active compression. This work purposes an active compression set capable of applying a cyclic compression at physiologically beneficial pressure gradients while improving on the prior art through utilizing a more efficient active compression system design while achieving a comparatively temperature independent design. Additionally, the achievable pressures gradients are an order of magnitude larger than those presented in prior art utilizing the same smart actuation technology. The design, modelling, fabrication, and testing of the novel smart active compression set are presented.

1.1 Scope of Work

This work was conducted as a division of the Lockheed Martin Corporation – Second Heart Project. The work presented over the course of this thesis will be focused on the active compression system. Although the design requirements are based on physiological testing performed by another team on the Second Heart Project, evaluation of the physiological effects of the active compression system is beyond the scope of this thesis. Additionally, the energy delivery method to power the active compression system will not be examined in this work. Finally, although a complete active compression system utilizes several “cuffs” connected from the ankle to the knee and actuated in series in order to induce the “milking” effect, this work will focus on the proof-of-concept of one cuff, termed an active compression set.

The scope of this thesis is explicitly on the engineering design, modelling, fabrication, and testing of a dielectric (DE) elastomer based active compression set. This includes the optimization and characterization of all the components that make up the active compression set in order to achieve a

final product that meets the requirements described by the physiology department. The major requirements to be present in the completed deliverable are stated below:

- System capable of achieving cyclic actuation with a pressure gradient of 10 mmHg uniformly around the circumference of a cylindrical test bed.
- A compressive pulse shape which matches that mandated by the physiology department (400 ms compression-relaxation pulse duration).
- Repeatable actuation.
- Relatively high power efficiency compared to prior art.
- Lightweight system.

1.2 Thesis Organization

This thesis will be structured as follows:

Chapter 2 – Background and Literature Review

This section will provide background information on the cardiovascular system in order to more thoroughly understand the potential effects of the project deliverable. Additionally, the existing state of the art on external compression will be examined in more detail. The major smart material actuation technologies that can potentially be utilized in an active compression system will be presented with a focus on DE actuators. Finally, the existing state of the art on dielectric elastomer based active compression will be examined in detail and its deeds and shortcomings described.

Chapter 3 – Design and Modelling

The novel DE active compression set design will be presented and both its components (belt mechanism and DE actuator) will be described in detail. The major design considerations will be described and analytical models describing the operation of the belt mechanism will be formulated.

Chapter 4 – Static Testing

This section will focus on static active compression set testing. The analytical models presented describing the belt mechanism will be validated experimentally. Additionally, a static actuation characterization of the DE actuators will be conducted and through utilizing the optimal system parameters, active compression set testing will be carried out.

Chapter 5 – Dynamic Testing

This section will include the modelling of the voltage input shape to match the required physiology output shape. Additionally, the "hold time" method will be introduced in detail and characterized. Dynamic DE actuator testing will be conducted, and through utilizing the optimal hold time and DE actuator parameters, cyclic active compression testing will be conducted and the required pressure gradient of 10 mmHg will be achieved.

Chapter 6 – Regenerative Powering System – Preliminary Analysis

This section will present the preliminary analysis and testing results of the regenerative powering system. The system attempts to reduce system power consumption through utilizing the charge stored in one capacitive element to charge another capacitive element. This method may be beneficial in future work where several active compression sets are connected and actuated in series to form a complete active compression system.

Chapter 7 – Conclusion and Future Work

The major thesis achievements and conclusions will be reiterated and discussed. Additionally, limitations of the current work will be presented along with recommendations for future work in this field.

Chapter 2
Background and Literature Review

2.1 Cardiovascular System

The cardiovascular system is essential for the survival of all the cells in the human body. It does this by maintaining the appropriate composition of the humans' internal environment with regards to fluid temperature, pH, and the concentrations of additional substances. The cardiovascular system circulates the blood in order to transport nutrients, oxygen, carbon dioxide, and other waste products [16]. The main components of the cardiovascular system are the heart, blood, blood vessels, and the lungs; with the heart acting as the main pump to promote blood circulation [17]. The cardiac cycle consists of the two major events that happen across the period of one heartbeat. During systole, blood is pushed through the arteries to the various organs as the heart muscles contract. In diastole, the ventricles fill with blood as the heart muscles relax [18].

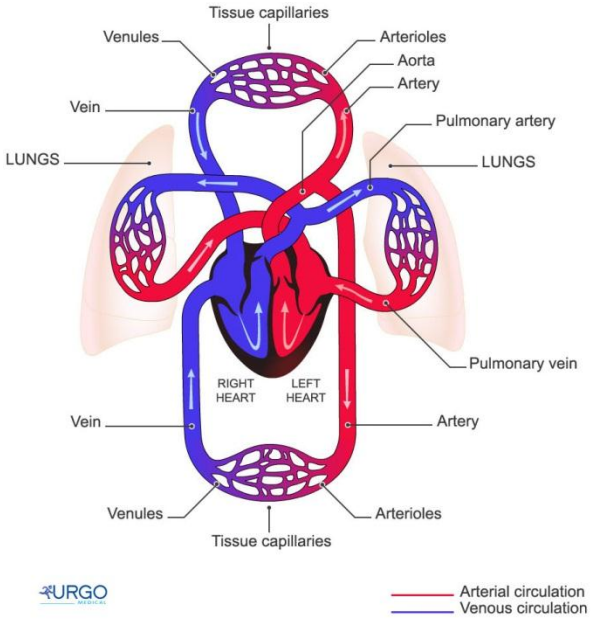

Figure 2-1. The cardiovascular system [19].

As shown in Figure 2-1, oxygenated blood is pumped out the left ventricle of the heart and through the aorta into arteries and small branches termed arterioles, moving into the capillaries where an exchange of nutrients, oxygen and other substances occurs with the body tissues [16]. This flow occurs from an area of higher pressure to an area of lower pressure due to the pumping of the heart. In

order to return the now de-oxygenated blood back to the heart through the veins, the pressure in the atria must be lower than the pressure in the veins. This is facilitated by the low pressure in the heart's atria during diastole and the skeletal muscle pump, which acts as a second heart [20]. The skeletal muscle pump, calf muscles or soleus, contracts thus counteracting the force of gravity on the blood and increasing the internal pressure in the veins to help push blood back up to the heart [20-22], as shown in Figure 2-2. The now deoxygenated blood travels through veins into the right atrium and the right ventricle. This blood is pumped through the pulmonary artery into the lungs where the blood is re-oxygenated and delivered back to the left ventricle to repeat the cycle [16].

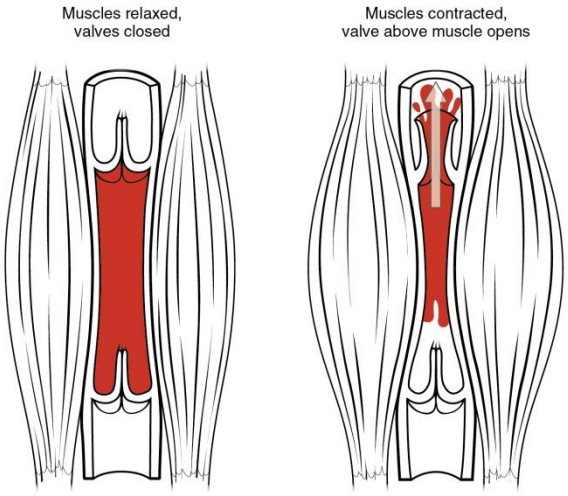

Figure 2-2. Skeletal muscle pumps method of operation [20].

2.2 Compression Therapy

Compression therapy is commonly used as a prophylaxis for the stasis of venous blood in the lower limbs and in turn the formation of a DVT. The stasis of venous blood may additionally induce chronic leg swelling, ulcerations, and edema [3]. DVT has been found to occur frequently in cases of patients undergoing surgery and in individuals of old age [5]. It was observed that 13% of non-surgical patients bedridden for eight days tested positive for markers that indicate DVT [23]. The formation of a DVT, and its associated symptoms, is a widespread clinical issue in the United States with approximately 250,000 new cases annually [24].

2.2.1 Passive Compression

Passive compression is commonly applied in the form of compression stockings and bandages. These compression garments function by compressing the lower limbs, specifically through incurring a pressure gradient along the length of the leg. The maximum compressive pressure is applied at the ankle and it is gradually decreased towards the knee or thigh. Passive compression garments squeeze the superficial veins in the lower limbs and direct flow from the veins to the deep system thus aiding in the return of blood from the lower limbs to the heart and in reducing venous blood pooling [25].

Compression garments may be knee or thigh high, and the applied pressure is a function of the mechanical properties of the garment and the wearer's limbs, along with the circumference of the wearer's limbs [14, 26]. In order for a compression garment to provide a potential benefit to the wearer, it must be sized and worn correctly. Compression bandages must be applied by a trained professional in order to incur the positive effects. On the other hand, compression stockings can commonly be purchased in a stock size based on the patients' foot size or calf and ankle circumference. While this provides the added benefit of an ease of application, incorrect application of the stocking can lead to a reverse-pressure gradient where the pressure is higher at the thigh than around the ankle. This has been found to lead to skin damage, patient discomfort, and in some cases, arterial thrombosis [3, 25, 27]. Graduated compression stockings are segmented into grades based on their maximum applied pressure (on the ankle). The grades are as follows by the European Commission of Normalization [28]:

- Grade I: Mild, 15 - 21 mmHg
- Grade II: Moderate. 23 – 32mmHg
- Grade III: Strong, 34 - 46mmHg
- Grade IV: Very strong, >49mmHg

Although the principle behind the operation of compression garments is generally agreed upon in the literature, several studies present opposing conclusions on the physiological effectiveness of compression garments [25, 29, 30]. Lord & Hamilton [25] shows that compression stockings in the 20-30 mmHg range only compressed the superficial veins when the wearer was supine, whereas they had no physiologically beneficial effect in standing individuals. On the other hand, several studies have found a benefit for graduated compression stockings in reducing leg edema during travel [29, 30].

Reviews of several published works suggest that compression garments have a minimal effect on athletes' performance during exercise [14, 26]. In a study examining the effects of lower limb passive compression on twelve healthy individuals, it was found that the load applied by the compression stocking can be found to vary largely across each wearing. Additionally, it was observed that compression garments exerting 15-25 mmHg reduced the volume of blood in the lower limbs, but did not incur an increased blood flow in the standing position [31]. The pressures applied by the compression garments and the position of the subject play an important role in determining the effectiveness of the garment [32]. Given the hydrostatic pressure due to gravity on the subject's blood in a standing position, a higher pressure will be required to narrow the vein diameter than that required for a subject in a supine position. It has been observed that a pressure of 30mmHg is required to begin narrowing the veins in a standing position [25]. It is evident from this array of results that the effectiveness of compression stockings for healthy individuals is contested in the literature.

2.2.2 Pneumatic Active Compression

Several studies have directly compared the effects of passive and active compression and have found active compression in the form of intermittent pneumatic compression (IPC) to have a more significant effect on improving physiological hemodynamic responses [4, 9, 10]. This is particularly evident in a study by Vanek [9], where it is presented that though utilizing IPC devices, the risk of DVT can be mitigated by 62% when compared to the placebo, and 47% when compared to passive compression stockings. A pneumatic active compression system generally consists of wrapping several air bladders around the leg that are inflated sequentially utilizing a pump [27]. This compression deforms the veins, which assists in reducing blood stasis and in emptying the deep veins in the lower extremities, which will in turn be filled again after deflation [27, 33, 37].

Pneumatic active compression systems can take many forms, where they may thigh or knee high, have varying numbers of cuffs, different applied pressures, and varied compression speeds [34]. An example of a knee high active compression system utilizing five cuff is shown in Figure 2-3. The applied pressure is a function of the properties of the skin, tissues, muscles, and vessels [33]. A study performed on 55 volunteers is presented by Tochikubo *et al.* [8] where active compression is applied using four air cuffs applying a sequential pressure from the feet to the thighs. This study also presents pulse synchronized compression during the diastolic period of the heart. It is shown that the peripheral vascular blood flow was increased in the lower limbs. There exist various analyses in the literature as to whether knee of thigh high compression is preferred. Results by Keith *et al.* [35]

conclude that there is an insignificant difference in peak blood flow velocity in knee and thigh high compression. On the other hand, Flam *et al.* [36] presents results showing that knee high compression is preferable to thigh high compression. There exist both low pressure-slow inflation and high pressure-fast inflation compression devices. A study completed on 22 healthy lower limbs and 11 lower limbs from subjects with venous insufficiencies found that the high pressure-rapid inflations compression incurred higher maximum blood velocities than low pressure–slow inflation [37].

Figure 2-3. Pneumatic active compression system with 5 compression cuffs.

2.3 Smart Material Actuation Technologies

Smart materials, also known as adaptive or intelligent materials, can be defined as materials that allow energy to be converted between several physical domains [38]. Smart materials can be separated into classes based on the specific physical domains that are coupled. Materials that exhibit a change in strain with temperature change exhibit thermo-mechanical coupling [39]. Electromechanical coupling exists when energy can be converted from the mechanical to the electrical domain and vice versa. The smart materials examined are shown in Figure 2-4 below, with their coupled domains shown. It can be seen that electromechanical materials exhibit two-way coupling, where an electric input is converted to a mechanical output, and a mechanical input can be converted to an electrical output.

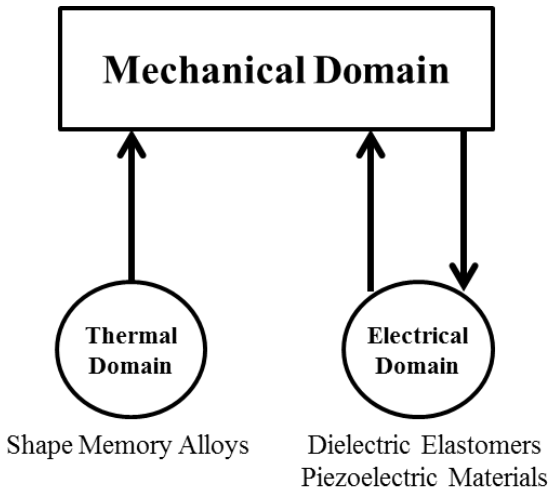

Figure 2-4. Examined smart materials and their coupled domains.

2.3.1 Piezoelectric Materials

As shown above, piezoelectric materials present an electromechanical coupling. These operate due to the electrical dipoles present in piezoelectric solids. A dipole can be presented as a two opposite charges separated with a pin in the middle [38]. Weiss domains are locations where the dipoles are aligned together, but the various Weiss domains are randomly oriented throughout the material. In order to align the various domains, poling through the application of a large electric field at a high temperature is conducted [40].

The direct piezoelectric effect is responsible for the generation of charge when a mechanical strain is induced in the material. With the application of a strain, the dipoles will rotate within the material and this movement will induce a charge flow. The converse piezoelectric effect is where mechanical strain is induced due to the application of an electric field to the material. The dipoles rotate upon being introducing to an electric field thus producing a strain in the material [38]. It is this mechanism that is utilized in actuation. Piezoelectric materials are the fastest responding smart materials of those presented in this thesis with a response time in the order of microseconds [38]. Additionally, given their high pressure and low strain outputs, piezoelectric actuators have found uses in various applications [41]. These applications include piezoelectric based micro-speakers [42] and motors [43]. Additionally, several applications such as atomic force microscopes [44] use them as a precision positioning device. On the other hand, due to their low strain capabilities, <0.1% [41], piezoelectric

actuators cannot be used effectively to apply uniform compression around a deformable object such as a human limb without incorporating a high order leveraging mechanism.

2.3.2 Shape Memory Alloys

Shape memory alloys (SMA's) are thermo-mechanical metallic alloys that can return to their initial form when they are heated beyond a given temperature. These materials have two stable phases which exist at a high temperature and at a low temperature respectively, where the crystal structures are found to vary. The material presents the austenite and the martensite structures at high and low temperatures respectively. After deformation due to loading, heat induces a material change from martensite to austenite, where it begins to recover its original form, even in the presence of an applied load. The transition in between the two structures is termed as the shape memory effect. These materials exhibit total strain recovery as long as the load applies a stress which induces a strain lower than the martensite yield strain, this is approximately 8.5% strain for NiTi alloys [45].

Some major advantages of utilizing SMA's includes their capacity to respond to changes in the environment, their lack of mechanical complexity, their high energy density (25 times greater than the density of electrical motors [46]), and their capability to lift more than 100 times their own mass [47]. On the other hand, SMA's have low controllability and accuracy. Arguably the largest issue with utilizing SMA's is their low actuation frequency. Given their thermal actuation, the speed of the response is directly related to the speed at which heat can be transferred into and out of the material. While the heating time can be reduced through utilizing joule heating, this method can potentially damage the material [48]. Through utilizing a fluid such as water with Glycol, the cooling time can be reduced by up to 100 fold [49]; however, this requires a complicated actuator design and still provides a relatively slow response when compared to similar piezoelectric and dielectric elastomer actuators. Finally, SMA actuators present very low energy efficiencies with a maximum theoretical efficiency of 10-15% [50], and efficiencies lower than 1% [51] in practical applications.

Moein & Menon and Holschuh *et al.* [52, 53] utilize SMA's in novel active compression system designs and achieve significant pressure gradients, with a maximum pressure change of approximately 20mHg during activation. However, the response time of the actuators remains an unsolved limiting factor that prohibits their use in a high-speed active compression system. It is shown in [52] that the utilized actuation system requires 0.94 and 19.25 seconds for the applied pressure to reach 80 and 95 percent respectively of its maximum actuation pressure value, with an

applied current of 150.3 mA. Additionally, SMA actuators' high power consumption, an example of which is shown in a morphing compression garment utilizing SMA actuators by Holschuh *et al.* [54], precludes their use as a low power active compression device.

2.3.3 Dielectric Elastomers

Similar to piezoelectric materials, dielectric elastomers (DE) exhibit electromechanical coupling. A DE comprises of a thin incompressible elastomer that is sandwiched between two electrode layers. Given the low modulus of the elastomer used as the dielectric, in the order of 1 MPa [55], a DE is in essence a compliant capacitor [56]. Dipoles, which consist of molecules carrying dipole moments or positively and negatively charged species, exist in the electrically neutral elastomer. Upon the application of an electric field, the various dipoles will align with their positive section oriented towards the lower potential and their negative section oriented towards the higher potential [55]. This in turn leads to a generated Maxwell stress, described by equation (1) which squeezes the elastomer in its thickness. Due to incompressible nature of the elastomer, it expands along the plane thus expanding in area and decreasing in thickness as displayed in Figure 2-5. Electrical energy is converted to mechanical strain energy as the distance between similar charges is increased as the elastomer increases in area, and the distance between opposite charges is decreased as the elastomer decreases in thickness [57].

$$p = \varepsilon_o \varepsilon_r \left(\frac{V}{d}\right)^2$$

$$E = \frac{V}{d} \qquad (1)$$

where p is the Maxwell stress that is generated ε_o is the permittivity of vacuum ($8.854 * 10^{-12}$ F/m), ε_r is the relative permittivity of the elastomer used, V is the voltage difference applied across the dielectric material, d is the thickness of the dielectric, and E is the induced electric field. The experimental validation of equation (1) can be found in a work by Kofod & Sommer-Larsen [58]. It is clear that the applied Maxwell pressure is proportional to the square of the applied electric field.

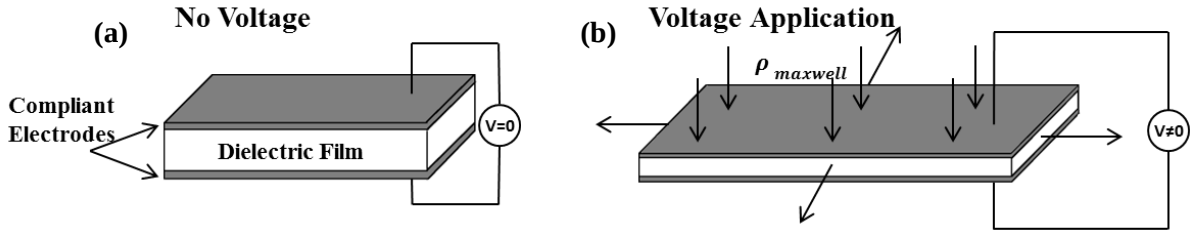

Figure 2-5. Activation method of DE. (a) No voltage applied. (b) Voltage applied.

The response of dielectric elastomer actuators have been characterized in various studies which have determined that DE actuators exhibit excellent actuation properties such as light weight, high strain outputs, high energy densities, quick response times, and low raw material costs [38, 56, 59]. Quantitative and qualitative assessments of the various actuation properties of DE actuators in comparison with the other smart material options are presented in Table 1 and Table 2 respectively. Due to the various desirable properties of DE actuators, this technology has been examined for a significant amount of potential applications. Goulbourne *et al.* and Goulbourne *et el.* [60, 61] analytically evaluate the use of a DE diaphragm as the active element in prosthetic blood pumps and present evidence that show that it could potentially prove advantageous over traditional artificial devices. Maffli *et al.* [62] fabricate and test a quick DE-driven tunable lens capable of operating for over 400 million cycles without failure. DE actuators have also been considered for MRI applications [63], braille displays [64], and biomimetic robots [65, 66]. These actuators have been utilized in several exciting configurations such as diamond [67], diaphragm, unimorph, bimorph [68], roll [69], and helical actuators [70].

2.3.3.1 Dielectric Materials

One of the critical design aspects for DE actuators is the elastomer used as the dielectric material, where both acrylic and silicone elastomers are prevalent in the literature. Some of the major parameters involved in the material choice include:

- Dielectric permittivity (ε_r): This is the ratio of the capacitance of a given capacitor using that dielectric material to the capacitance of a capacitor with vacuum as its dielectric. As shown in equation (1), this parameter directly affects the magnitude the generated Maxwell Stress, where a larger dielectric permittivity value is desired.
- Dielectric strength (E_b): The dielectric strength is the maximum electric field that the dielectric can sustain before breakdown. Its effects are also presented in equation (1), where

the generated Maxwell Stress is proportional to the applied electric field. Therefore, a material that can sustain large electric fields is desired.

- Visco-elasticity: A high material visco-elasticity leads to increased viscous losses and slower response times [71]; therefore, materials with low visco-elasticity are desired.
- Mullins effect: This is the materials' stress-strain curve dependence on the maximum encountered loading. In particular an irreversible softening of the material as a new maximum strain value is induced [72].
- Lifetime: The lifetime is largely a function of the fabrication method and testing environment [55], whereas both factors are influenced by the elastomer used.

Acrylic elastomers present the advantage of having higher dielectric permittivity's (ranging from 2-8) when compared to silicone elastomers (2-3), this in turn leads to actuators utilizing acrylic elastomers exhibiting higher energy densities [73]. Acrylic elastomers have therefore been shown to achieve higher strains [68]. On the other hand, DE actuators with silicone elastomer dielectrics produce more repeatable actuation. Additionally, they present minimal Mullins effects and have been shown to operate up to 400 million cycles without failure [55, 62]. Furthermore, silicone elastomers are significantly more efficient than their acrylic counterparts given their lower visco-elasticity and therefore minimal viscous losses [71]. In addition, silicone elastomers can be operated at a larger temperature range [74], and are significantly better suited for high frequency cyclic actuation due to their relatively low visco-elasticity. This is shown experimentally in Molberg *et al.* [71] where it was observed that the strain output of a VHB (acrylic) elastomer decreased from 3.55% at an actuation frequency of 1 mHz to 0.03% at an actuation frequency of 1 Hz. In contrast, the PDMS (silicone) elastomer strain output decreased from 1.22% at 1 mHz to 0.82% at 1 Hz. A thorough review of the various silicone elastomers used in DE actuators is presented in Madsen *et al.* [55].

2.3.3.2 Electrodes

Electrodes are crucial to the operation of DE's since they allow charges to be quickly added and removed from the dielectric material's surface. According to Pelrine *et al.* [75], "The ideal electrode would be highly conductive, perfectly compliant and patternable, and be made thin relative to the polymer thickness." Whereas Michel *et al.* [76] describes that "A good electrode material should retain conductivity with strain, be compliant, have a low modulus of elasticity and low cost, be easy to fabricate, have extended strain cycling and resistance to wear, and should not delaminate." To date, there is no agreed upon "ideal electrode material", where all available solutions present some

shortcomings. Electrodes based on carbon particles are most prevalent in the DE literature. These carbon based electrodes consist in three forms: carbon powder, carbon grease, and conductive elastomers [77].

Carbon powder electrodes have the advantage of being perfectly compliant due to their powder form. However, they present issues in ease of handling, maintaining conductivity at high strains [78], and electrode lifetimes due to the possibility of detaching from the elastomer surface. Carbon grease electrodes consist of carbon particles bound into a grease mixture and spread on the elastomer surface. These electrodes are easier to handle, and maintain conductivity at higher strains. On the other hand, actuators utilizing carbon grease electrodes tend to have shorter lifetimes due to the possible drying of the grease or diffusion in the dielectric membrane over time [77]. Elastomeric electrodes consist of carbon powder mixed in an elastomer matrix; the cured combination forms a conductive elastomer. These electrodes solve the majority of problems associated with the aforementioned electrode types; however, present the issue of no longer being perfectly compliant due to the stiffness of the cured elastomer [76]. Pelrine *et al.* [75] states that these electrodes are most effective when they can be made in a thickness that is negligible compared to the thickness of the dielectric layer. This issue has been shown to be reduced through utilizing appropriate electrode mixtures and casting/electrode deposition methods in [79].

Metal electrodes are also commonly found in the literature. Choi *et al.* [80] developed an active frequency selective surface utilizing a dielectric elastomer incorporating stretchable silver nanowire electrodes. Benslimane *et al.* [81] analyses several DE actuators which utilize compliant metal electrodes and present good response times, lifetimes, and achievable stresses and strains. While these works present the potential of DE actuators utilizing metallic electrodes, there remain significant disadvantages to this method that must be addressed. First, due to the relatively high stiffness of metals compared to the dielectric materials used, even a thin electrode will add significant stiffness to the elastomer thus reducing the actuation potential. This is shown in Rosset *et al.* [82], where the stiffness of a 30.6 μm PDMS film was increased from 0.77 – 4.2 MPa simply through the addition of an 8 nm sputtered gold electrode layer. Additionally, since the limit of elasticity for metals is fairly low at 2-3%, creative techniques must be utilized in order to design electrodes that maintain conductivity at high strain values [77].

Additional studies have shown encouraging advances in fabricating and depositing thin film electrodes which allow the actuator to 'self-heal' after suffering dielectric breakdown, therefore extending the life of the actuator beyond what is currently possible [76, 83].

2.3.4 Summary

The properties shown in Table 1 are obtained from [38, 45, 57, 84]. Given that the active compression system is attempting to mimic the effects of the skeletal muscle pump, the natural muscle values are taken as a benchmark, as displayed in Table 2. It can be seen that both SMA and Piezoelectric actuators fall short in their achievable strain when compared to natural muscles. Additionally, SMA's have relatively low efficiencies and actuation bandwidths. On the other hand, as described by Bar Cohen and Pelrine *et al.* [56, 73], dielectric elastomer actuators are most similar to natural muscles and have the most well-rounded performance characteristics. Therefore, they are commonly referred to as "artificial muscles". Given that DE actuators meet all the required characteristics, they are selected as the actuation technology for this application.

Table 1. Summary of actuation methods' quantitative performance characteristics.

Actuator/Property	Strain (%)	Actuation Pressure (MPa)	Efficiency (%)	Bandwidth (Hz)	Work Density (J/cm^3)
Natural Muscle	20-40	0.1-0.8	35	2-173	0.008-0.04
Shape Memory Alloy (NiTi)	<8	200	3	0.1-3**	>1
Piezoelectric	0.1	35	50	5000	0.035
Dielectric Elastomer	1-10%	0.1-3	3	>100	0.01-0.15

**Depends largely on the method of heating and cooling [48].

Table 2. Qualitative analysis of actuators' performance characteristics compared to that of natural muscle.

Actuator/Property	Strain	Actuation Pressure	Efficiency	Bandwidth	Work Density
Natural Muscle	Good	Good	Good	Good	Good
Shape Memory Alloy (NiTi)	*Average*	Good	*Bad*	*Bad*	Good
Piezoelectric	*Bad*	Good	Good	Good	Good
Dielectric Elastomer	Good	Good	Good	Good	Good

2.4 DE Active Compression – Prior Art

There currently exists two published works focused on the design and testing of a DE based active compression bandage [85, 86]. Pourazadi *et al.* [85] Demonstrates the ability to achieve a maximum pressure gradient of 1.05 mmHg through the use of a single-layered DE strip actuator which is connected around a leg-like test bed using Velcro®. The compression bandage is stretched and connected around the test bed leading to an initial compressive pressure. Given the planar expansion of DE actuators with voltage application, the applied compressive pressure is reduced during actuation. The maximum compressive pressure is re-attained when the voltage is removed resulting in the actuator decreasing in length and tightening around the test bed. Although a significant contribution, the major shortcomings of these papers are listed below:

1. *The method of applying active compression – Active compression bandage design*

   As described above, maximum compression is only attained upon removal of the applied electric field leading to the DE actuator contraction. This is highly disadvantageous for an application that requires the stocking to be in a low pressure state for the majority of the time followed by a quick compression pulse. That is due to the fact that this would necessitate that the actuator remain charged for longer periods of time and only discharge during compression. This can potentially

incur larger power consumption due to current leakage [59, 83], and reduced DE actuator lifetimes due to continuous stress on the actuator [87].

In addition to that, given the nature of wrapping the DE actuator around the test bed with an initial pre-stretch, the initial mechanical pressure can only be controlled by varying the stretch ratio. Most DE actuators require to be stretched to operate effectively, thus this is a major limitation on the potential for the scaling up of the size of said actuators to achieve higher pressure variations since the initial mechanical pressure will be too high due to the increased actuator stiffness at a given stretch ratio. Pourazadi *et al*, [85] Shows a 5.2% pressure drop due to actuation; therefore in order to achieve pressure gradients in the order of 10's of mmHg an unreasonable initial mechanical pressure must be applied on the test bed. Similarly, Pourazadi *et al.* [86] predicts a maximum pressure drop of 10% attained with an initial mechanical pressure of 45mmHg, which is reduced to 5% at an initial mechanical pressure of 22.5 mmHg. Finally, the active compression bandage utilizes a single layer DE actuator with a dielectric thickness of 1.34 mm. In order to achieve the Maxwell pressures required to incur a pressure variation of 1.05 mmHg, a high voltage of 13 kV must be applied which presents electrical safety and power supply concerns.

2. *The results obtained*

Pourazadi *et al.* [85] achieves minimal pressure gradients with actuation (1 mmHg), which is an order of magnitude lower than what is physiologically required to incur a measureable change in lower extremity blood flow. Additionally, voltage is applied using static voltage steps, whereas cyclic actuation is not evaluated.

Chapter 3
Design and Modelling

3.1 Active Compression Set Design

In order to apply DE based compression in a more effective method than currently used in the state of the art, an innovative active compression set design was conceptualized and fabricated. This consists of a multi-layered DE strip actuator connected in conjunction with a belt mechanism as shown in Figure 3-1. This belt mechanism allows the system to utilize the intrinsic nature of the DE actuator, which expands with voltage application, in order to apply compression directly with the voltage application. This is done through wrapping the belt mechanism around the cylindrical test bed, where it "rolls into itself" similar to a belt. Upon pushing the ends away from each other, the belt mechanism tightens around the test bed and a compression is applied. In order to initially tighten the belt mechanism around the test bed and incur a compressive pressure, compression springs are connected in a compressed state between the ends of the belt mechanism leading to spring forces, $F_{Spring.}$ Through stretching the DE actuator and connecting it in tension between the ends of the belt mechanism, the pushing force of the springs is counteracted and the compressive pressure is reduced. Upon application of a voltage to the DE actuator, it elongates in length thus reducing the counteracting tensional force F_{DE}, and leading to an increased compressive pressure on the cylindrical test bed.

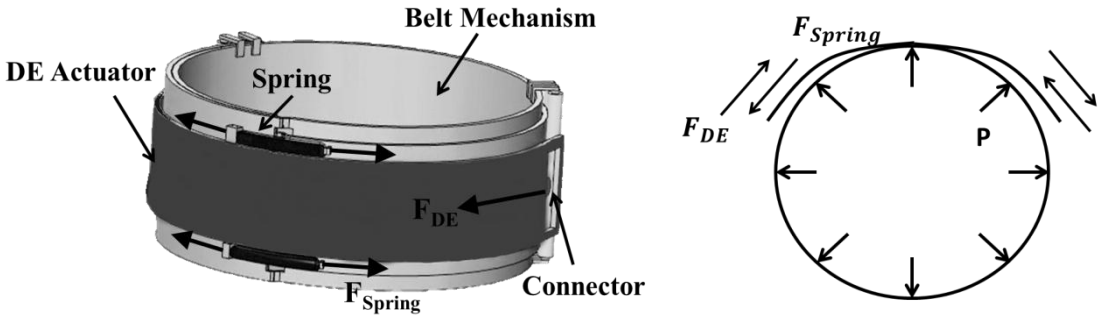

(a) **(b)**

Figure 3-1. (a) Active compression set. (b) System cross section free body diagram.

3.1.1 Belt Mechanisms

In order to function efficiently, the Belt Mechanism must be capable of bending with the contour of the leg and must be made of a material with little stretch exhibited to limit losses during actuation. To fulfill these requirements, a cured composite carbon-fibre strip of 0.6 mm thickness is initially used due to its high stiffness, low density, and flexibility. Connection points were then attached to the body to allow for efficient connection of the springs and DE actuator to the belt mechanism. Upon rolling the strip into itself, two identical steel compression springs with rate constants (the product of the spring stiffness and its free length) of 65 N are connected in compression at the connection points on both ends of the belt mechanism. The compressed spring length is constant and is defined by the distance between the fixed connection points on the belt mechanism and the radius of the non-deformable cylindrical test bed. Springs with various free lengths are utilized to induce different initial pre-compressions. The fabricated Original Belt Mechanism (OBM) with the attached compression springs is shown in Figure 3-2. The system weighs a total of 99 g.

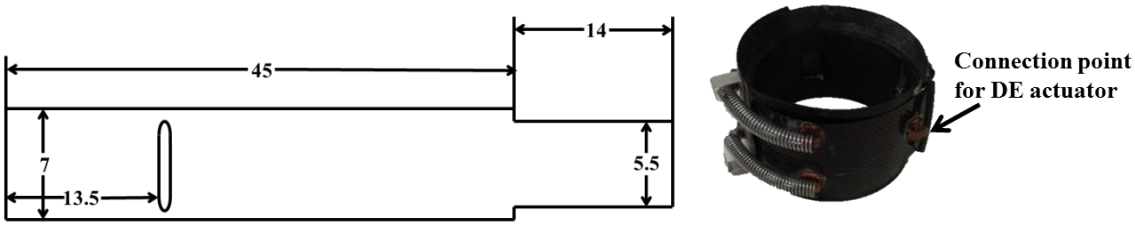

(a) **(b)**

Figure 3-2. (a) Belt mechanism design, all units in cm. (b) Fabricated belt mechanism with attached compression springs.

One of the major advantages of the belt mechanism is that the initial pre-compression experienced by the test bed before voltage application can be controlled and optimized as per the user's needs. Rather than simply relying on the pre-stretch and stiffness of a DE actuator wrapped alone around the cylindrical test bed to determine the initial pre-compression, through varying the spring lengths and in turn the spring forces F_{spring}, the pre-compression can be set at any value. An analytical expression defining the initial pre-compression as a function of spring free length and other parameters is formulated in the coming section, and is validated experimentally in the Belt Mechanism Validation section.

In order to further improve on the belt mechanism design, a Soft Belt Mechanism (SBM) was designed and fabricated. The SBM operates with the same principle as the OBM but is made out of Kevlar fabric thus allowing it to completely take the shape of the test bed/leg. Additionally, the high modulus of Kevlar®, comparatively low density, decent water and moisture resistance, and excellent abrasion resistance [88], make it an ideal material choice for a robust ambulatory active compression mechanism. The free ends of the Kevlar® fiber strip are stitched in order to prevent fraying and fixed connection points are fabricated in the belt mechanism to allow connection to the DE actuator and compression springs. Furthermore, it is designed in order to be as thin and light as possible, where the SBM with the springs attached weighs 47 g as opposed to the 99 g weight of the OBM with the springs attached. The compression springs used in the SBM have a 3 mm outer diameter and are therefore very flexible, thus reducing the size and allowing the Kevlar to cushion the region between the test bed/leg and the springs. Finally the Kevlar fabric body of the SBM allows for a "breathable" design and in turn further improves on the ergonomic aspects in terms of a final product. The SBM is shown in Figure 3-3.

Figure 3-3. Soft belt mechanism with attached compression springs.

The major advantages of the novel belt mechanism design can be summarized as follows:

- Compression applied directly with the application of a voltage.
- Longer DE actuator lifetime and less leakage current due to less charging time.
- Initial mechanical pre-compression before voltage application can be optimized as per the user requirement while maintaining optimized DE actuator pre-stretch.
- Effectively insulates individual from the high voltage DE actuator.

3.1.2 Dielectric Elastomer Actuators

As previously mentioned, elastomer choice is a critical aspect in DE actuator design. While acrylic elastomers have been shown to achieve higher strains [68], silicone elastomers are better suited for cyclic applications due to their relatively low viscoelasticity and higher efficiencies [71, 84]. For these reasons, along with several others outlined in the Dielectric Elastomers Section, all DE actuators in this work are fabricated with silicone elastomers as the dielectric of choice. In order to achieve the high actuation forces required to incur the physiologically beneficial pressure changes during active compression, multi-layered DE actuators are fabricated, where the actuation force is magnified as the number of layers increases. The fabrication process is executed in a clean room environment in an effort to reduce external contaminants which may have a detrimental effect on actuator lifetime and effectiveness.

A RS silicone mixture cast in-house at a 100 μm thickness is compared to a 50 μm thick Wacker Elastosil 2030 film in the Results section and it is determined that the Wacker film can sustain a higher electric field before dielectric breakdown; therefore, the Wacker film is utilized for all subsequent testing. This work will present both actuators fabricated with carbon grease and elastomeric electrodes. Carbon grease electrodes have the advantage of being compliant, readily available, and of low cost. However, they present a difficulty in handling when fabricating multi-layered actuators, and actuators fabricated with carbon grease electrodes exhibit shorter lifetimes [77]. On the other hand, elastomeric electrodes provide ease of fabrication for multi-layered actuators due to the ease of stacking several layers uniformly. It is, however, important to note that these electrodes are not compliant and therefore add inactive stiffness to the actuator therefore reducing the achievable actuation outputs [76]. Additionally, these electrodes must be fabricated in house and are not commercially available. They consist of a conductive carbon black and silicone mixture dissolved in a solvent and cast with a wet thickness of approximately 100 μm. The fabrication processes for both types of actuators are described below:

3.1.2.1 Elastomeric Electrode based DE Actuator Fabrication

The fabrication process for multi-layered DE actuators utilizing elastomeric electrodes begins with casting the elastomeric electrode to a 100 μm wet thickness on top of transfer paper. Following which, the cast electrodes and the dielectric material are laser cut to the required size. Using a thin layer of silicone, the dielectric and electrode layers are bonded together. This is repeated for every layer where each dielectric layer is sandwiched by two electrode layers. The electrode is cut to be of

smaller width than the elastomer in order to create a "buffer region" and reduce the possibility of a short circuit forming across layers. Finally, acrylic end pieces are attached to the fabricated DE actuator as shown in Figure 3-4(a) to allow a secure connection to the belt mechanism. One of the major complications in manual multi-layered DE actuator fabrication is the inherent difficulty in aligning a large number of electrode and dielectric layers directly atop one another. Figure 3-4(b) shows the dimensional parameters of the actuators and provides a visual representation of the buffer region (difference between total and active width).

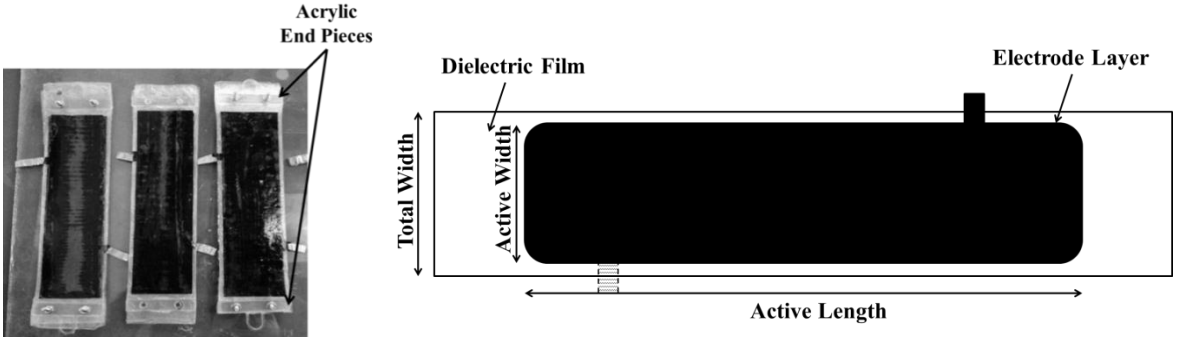

(a) **(b)**

Figure 3-4. (a) Fabricated DE actuators. (b) DE actuator design drawing.

3.1.2.2 Carbon Grease based DE Actuator Fabrication

The clean room fabrication process for carbon greased based DE actuators is similar to that utilizing the elastomeric electrodes, in that several layers are stacked atop each other and bonded together to form a multi-layered actuator. However, the method of placing the electrode layer differs where a shadow masking method is undertaken for the carbon grease electrodes. A shadow mask is created by utilizing a laser cutter to cut out the required shape into masking tape, following which the shadow mask is placed over the dielectric layer. The exposed section of the dielectric material is coated with a thin layer of carbon grease as shown in Figure 3-5(a). Following which, a conductive elastomer strip cast at 100 µm wet thickness is placed at the boundary of the electrode to form an external electrical connection point; this is shown in Figure 3-5(b). This process is repeated several times with several layers stacked atop each other and bonded together with a thin layer of silicone to form a multi-layered actuator. Similarly to the DE actuators with elastomeric electrodes, the width of the coated section is made smaller than the total width of the dielectric film to prevent the grease from leaking at the edges and forming a short circuit across layers. Furthermore, in order the insulate the electrode

layers from the environment, all fabricated actuators are encapsulated by a dielectric layer on each face, these layers only have an electrode on one side and are therefore inactive.

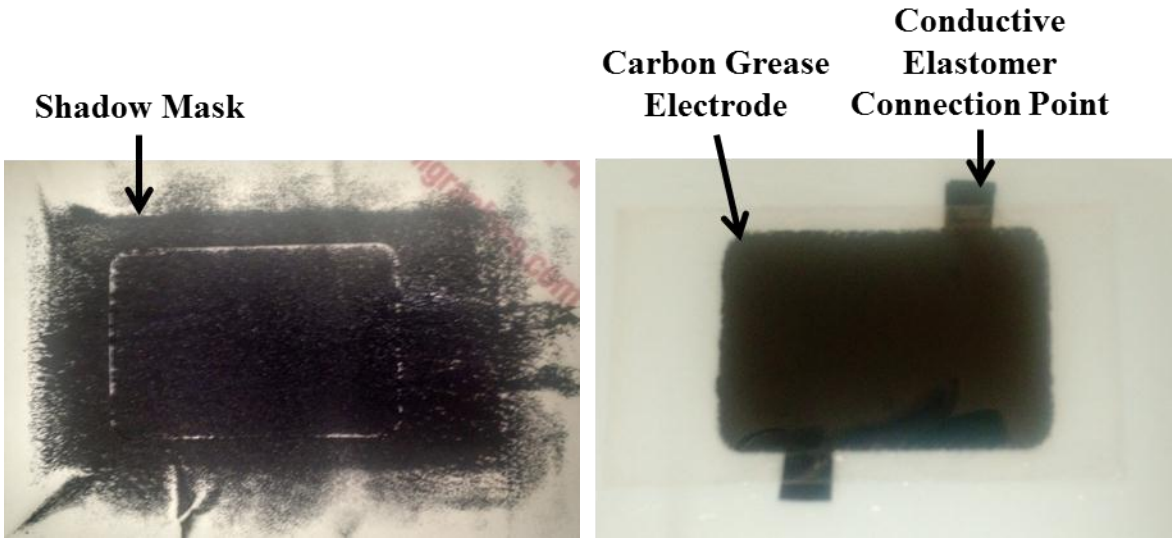

(a) **(b)**

Figure 3-5. (a) Shadow masking in DE actuator fabrication. (b) Dielectric layer with electrode following shadow masking.

3.2 Modelling

This section describes the analytical modelling of the belt mechanisms and dielectric elastomer actuator. In this section, it is assumed that the losses due to friction between the belt mechanism and the test bed are negligible. Additionally, it is assumed that the test bed is a non-deformable cylinder and the DE actuator exhibits linear elastic behavior for the stretch ratios utilized.

3.2.1 Belt Mechanism

The tangential force can be related to the incurred radial pressure, shown in Figure 3-6, by the Hoop Stress equation.

$$F_t = Prw \tag{2}$$

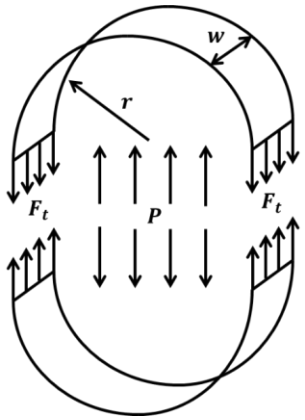

Figure 3-6. Hoop stress diagram.

F_t is the aggregate tangential force which is applied on either end of the belt mechanism, P is the incurred radial pressure test bed, r is the radius of the test bed, and w is the width of the belt mechanism. The tangential force is found from the counteracting forces of the springs and DE actuator as follows,

$$F_t = F_{sp} - F_{DE} \tag{3}$$

where the force applied by the two springs is:

$$F_{sp} = 2c(1 - \frac{L_s}{L_{os}}) \tag{4}$$

$$k = \frac{c}{L_{os}} \tag{5}$$

In the above equations, c is the rate constant of the springs, L_{os} and L_s are the free and compressed spring lengths respectively, and k is the spring constant. F_{DE} is determined by the equilibrium between the mechanical tension due to pre-stretch, F_m , and the tension relaxation due to actuation, F_e, produced upon the voltage application.

$$F_{DE} = F_m - F_e \tag{6}$$

Through combining equations (2) to (6) a relationship for the applied pressure P is found. The change in the spring length with the DE activation is assumed to be negligible due to the non-deformable nature of the test bed.

$$P = \frac{2c(1 - \frac{L_s}{L_{os}}) - (F_m - F_e)}{rw} \tag{7}$$

Before actuation, $F_e = 0$, and the pre-compression in the system reduces to,

$$F_e = 0 \rightarrow P_o = \frac{2c(1 - \frac{L_s}{L_{os}}) - F_m}{rw} \tag{8}$$

From equation (8), it can be seen that by changing the spring free lengths and stiffness's, any value for initial pre-compression may be obtained for any initial mechanical force, F_m. The change in pressure can be determined by the tension relaxation due to actuator activation as shown in equation (9). This increase in the radial pressure is proportional to the tension relaxation of the DE actuator upon voltage application.

$$P = P_o + \frac{F_e}{rw} \longrightarrow \Delta P = \frac{F_e}{rw} \tag{9}$$

3.2.2 DE Actuator

Given the high ratio of bulk to shear modulus of the elastomeric dielectrics used, the DE actuators are assumed to be incompressible in nature [89]. Thus, the Poisson's Ratio approaches a value of 0.5 and the following holds:

$$\lambda_{mi} = \frac{l_i}{l_{io}} \tag{10}$$

$$\lambda_{m1}\lambda_{m2}\lambda_{m3} = 1 \tag{11}$$

In equations (10) and (11), $\lambda_{m1}, \lambda_{m2}, \lambda_{m3}$ are the initial mechanical stretch ratios in each of the length, width, and thickness directions respectively, l_{io} is the initial dimension of the actuator, and l_i is the dimension after pre-stretch. Uniaxial tensile tests are performed on a number of fabricated actuators in order to characterize their stress/strain relationships. Tests were conducted using an INSTRON 4465 machine. The actuators were found to exhibit linear stress/strain behavior for strains smaller than 40%, as shown in Figure 3-7. Given that the stretch ratios utilized in this work fall below 30%, the actuators are assumed to exhibit a linear stress/strain relationship. More accurate models to account for the non-linearity at higher strains, such as the Ogden hyper elastic model are accessible in the literature [90].

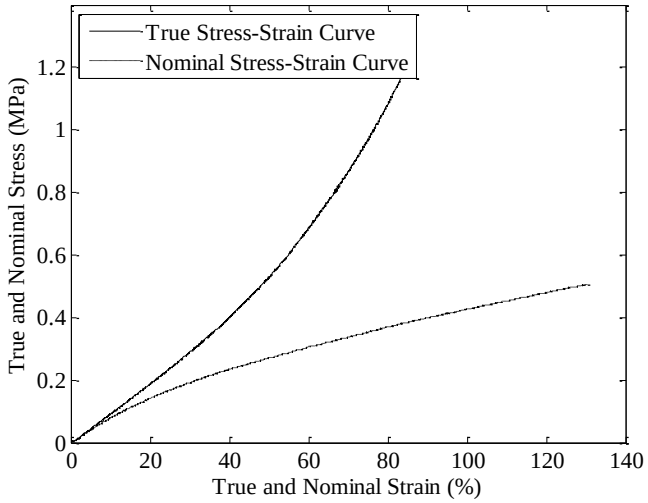

Figure 3-7. True and nominal stress-strain plots for fabricated actuator.

The longitudinal stress in the actuators due to the initial pre-stretch can be found using,

$$T_m = Y(\lambda_{m1} - 1) \tag{12}$$

where Y is the Young's Modulus of the actuator. The subsequent width and thickness of the DE actuator after pre-stretch can be found using the incompressibility assumptions:

$$d = \frac{d_o}{\sqrt{\lambda_{m1}}}$$
$$W = \frac{W_o}{\sqrt{\lambda_{m1}}} \tag{13}$$

Where W_o and d_o are the initial width and thickness of the DE actuator before pre-stretch respectively. Equations (12) and (13) can be combined to obtain the mechanical tension due to pre-stretch in the longitudinal axis.

$$F_m = YW_o d_o \left(1 - \frac{1}{\lambda_{m1}}\right) \tag{14}$$

Substituting equation (14) into (8), an equation defining the relationship for the initial pre-compression due to the force of the spring and DE stiffness, dimensions, and pre-stretch is obtained.

$$P_o = \frac{2c(1 - \frac{L_s}{L_{os}}) - YW_o d_o \left(1 - \frac{1}{\lambda_{m1}}\right)}{rw} \quad (15)$$

3.3 Summary

This chapter presents the novel design of an active compression set consisting of a belt mechanism used in conjunction with a DE actuator. This design presents the advantage of allowing active compression to be applied directly with voltage application. Additionally, the initial mechanical pre-compression exerted by the compression set before actuation can be optimized through varying system parameters. Analytical equations characterizing the operation of the active compression set and the initial pre-compression are formulated and will be validated in the Belt Mechanism Validation section of this work.

Additionally, due to their numerous advantages for cyclical actuation, silicone elastomers are chosen over acrylic elastomer for actuator fabrication. Finally, the two electrode types used in this work, elastomeric electrodes and carbon grease electrodes, are presented and their respective fabrication methods are described.

Chapter 4
Static Testing

This chapter will present the results of the Belt Mechanism Validation testing, static DE actuator testing, and static active compression set testing.

4.1 Methods

4.1.1 Actuators

Actuators are named based on the number of active layers they contain, and the elastomer used as the dielectric. Actuator A6-100R contains six active layers and utilizes 100 µm thick cast RS silicone as the dielectric while actuator A14-50W has fourteen active layers and utilizes 50 µm Wacker silicone film as the dielectric. An active layer is a dielectric layer which has an electrode on both faces, allowing it to actuate with the application of a voltage difference. In-active or passive layers are those dielectric layers which do not have an electrode on both faces. Each actuator contains an inactive layer on the top and the bottom face of the completed actuator in order to electrically insulate it. While these layers are crucial for the safe operation of the actuator, they add an inactive stiffness to the actuator thus reducing its achievable strain outputs during actuation. All actuators in this chapter were fabricated with elastomeric electrodes, where the fabrication method is described in detail in the Design and Modelling Chapter.

Two groups of actuators were fabricated for different purposes. The first group, which consisted of two actuators, A6-100R and A6-50W, was fabricated for the purpose of comparing between the two dielectric materials presented above. The critical aspects examined in this comparison were dielectric breakdown strengths and achievable strains. Additionally, the first set of actuators was utilized to determine the strain output variation at different stretch ratio's and the induced creep during cyclic actuation. Both actuators have six active layers and the same dimensions as shown in Table 3.

The second set of actuators, consisting of actuators A8-50W and A14-50W, was fabricated in order to characterize the actuators' force-strain behavior and to test the complete actuation set consisting of the belt mechanism used in conjunction with an actuator. These actuators were both fabricated using the 50 µm Wacker silicone film; however, they have a different number of active layers. They possess a larger width and more active layers than those of the first set in order to exhibit larger force changes with DE activation and in turn are utilized to incur larger pressure variations during active

compression testing. Two additional actuators, A12-50W and A30-50W, were fabricated and suffered catastrophic failure immediately during testing. The reasons behind the actuators failures are outlined in the Actuator Failure Section of this chapter.

Table 3. DE actuators fabricated for static testing.

Actuator Name	Active Length (mm)	Active Width (mm)	Total Width (mm)
A6-100R	115	22	30
A6-50W	115	22	30
A8-50W	170	42	46
A14-50W	70	42	50
A12-50W (Breakdown)	170	42	46
A30-50W (Breakdown)	170	42	46

4.1.2 Test Setups

Several test setups are utilized in order to characterize the DE actuator response, validate the belt mechanisms analytical formulations, and test the active compression set. Throughout this chapter, the actuation voltage is applied using an EMCO G60 (0-6kV output) DC-DC voltage amplifier connected to an EXTECH 382275 power source. Additionally, as recommended by Carpi *et al.* [89], the DE actuation outputs are only measured after allowing the actuator adequate time to reach a steady state with its pre-stretch. This is due to creep exhibited directly after connecting the actuator with an initial stretch ratio.

The data required to define to optimal actuator parameters to be used during full system testing is obtained through actuator characterization. Three test setups are utilized to characterize the DE actuators' free strain, blocked force, and force-strain response:

1) Free strain setup (Figure 4-1(a)): This test setup involves hanging the actuator at one end and attaching masses to the free end to induce various initial pre-stretch ratios. A voltage difference is applied and the ensuing displacement is measured with an Electrotec IDS-70 laser displacement sensor as shown in Figure 4-1(a). This test setup is utilized in order to directly compare between the two dielectric materials in question, to examine the effects of the initial stretch ratio on actuation free strain output, and to characterize the creep effects introduced during actuation and the repeatability of cyclic actuation.

2) Blocked force and stress/strain test setup (Figure 4-1(b)): In order to characterize the blocked force of the actuators, a test setup is utilized where the DE actuator is attached at one end to a fixed point and at the other end to a Chatillon DFXII force gauge with an adjustable end piece. The initial pre-tension is recorded, and the ensuing tension relaxation with voltage application is determined. In characterizing the stress-strain relationship, the actuator pre-stretch is varied at increments using the force gauge adjustable end piece, where the end displacements are measured using a Keyence Il100 laser sensor through measuring the displacement at the connection point to the actuator. The change in force and strain are measured from the pre-stretch position.
3) DE actuator and spring test setup (Figure 4-1(c)): This test setup provides details of how the DE actuator reacts in a situation where it is connected in conjunction with a spring, in a scenario similar to the belt mechanism. The test setup involves the DE actuator connected at several pre-stretch values between a fixed point force gauge (Chatillon DFXII) and a spring, which is in turn connected to a fixed base. Upon application of a voltage to the DE actuator, it expands resulting in a measureable tension relaxation and an increase in length. The elongation of the actuator is measured using a Keyence Il100 laser sensor.

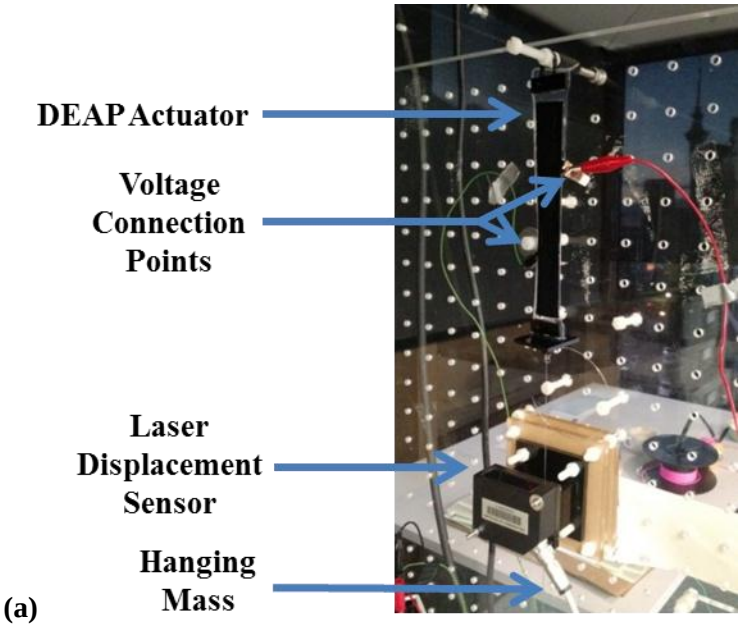

(a)

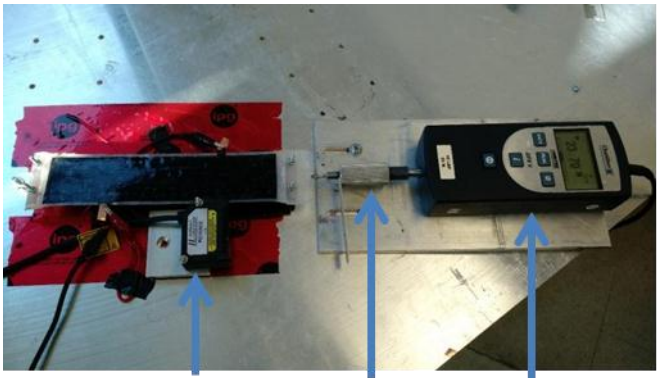

(b)

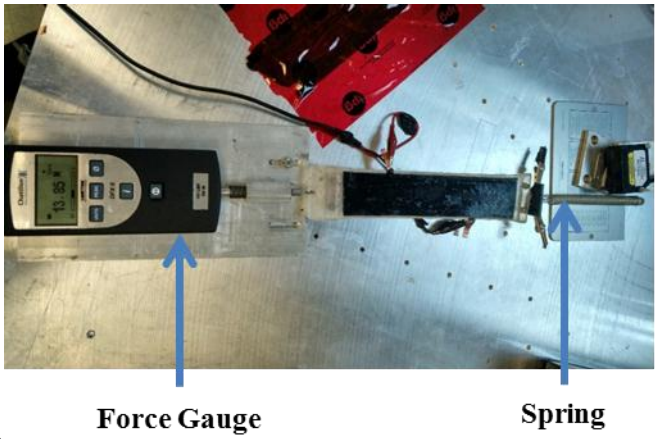

(c)

Figure 4-1. (a) Free strain test setup. (b) Force-strain and blocked force test setup. (c) DE actuator and spring test setup.

The second series of tests are conducted in order to validate the analytical equations defining the belt mechanisms' operation and to test the response of the active compression set consisting of the belt mechanisms connected along with a DE actuator. These tests are conducted around a PC-ABS alloy 3D printed test bed shown in Figure 4-2(a). The test bed has cut out sections to allow mounting of a piezoresistive-based force sensor (Honeywell FS01) capable of outputting an electrical signal to a LABVIEW controlled DAQ. The following test setups are utilized:

1) Belt mechanism tension relaxation validation setup (Figure 4-2(b)): This test setup is used to validate equation (9) which relates the change in the applied pressure on the test bed to the actuator tension relaxation. A silicone tube is used to mimic a DE actuator and is connected

in tension to both ends of either belt mechanism identical to the way the DE actuator would be mounted. The tension is varied and the ensuing radial pressure applied to the test bed is measured. The tension in the silicone tube is measured accurately using a load cell mounted at the connection point of the silicone tube to the belt mechanism. This test setup also allowed the pressure distribution throughout the circumference of the test bed to be measured by placing a piezo-resistive sensor (Interlink Electronics FSR 402) at various locations between the belt mechanism and the test bed.

2) Belt mechanism pre-compression validation setup (Figure 4-3(a)): In order to validate equation (8), the DE actuator is connected at a fixed stretch ratio in conjunction with the OBM around the test bed. Springs of various free lengths connected to the system and each incurred pre-compression value is recorded. This system is compared to the scenario where a DE actuator is connected with a given stretch ratio directly around the test bed (without the belt mechanism) as shown in Figure 4-4.
3) Active compression testing (Figure 4-3): This test setup involved connecting a DE actuator to the OBM and the SBM. The change in radial pressure upon DE activation can be documented and used to validate the effectiveness of the active compression sets. Additionally, this test setup allows for a direct comparison between the active compression sets utilizing the OBM and the SBM.

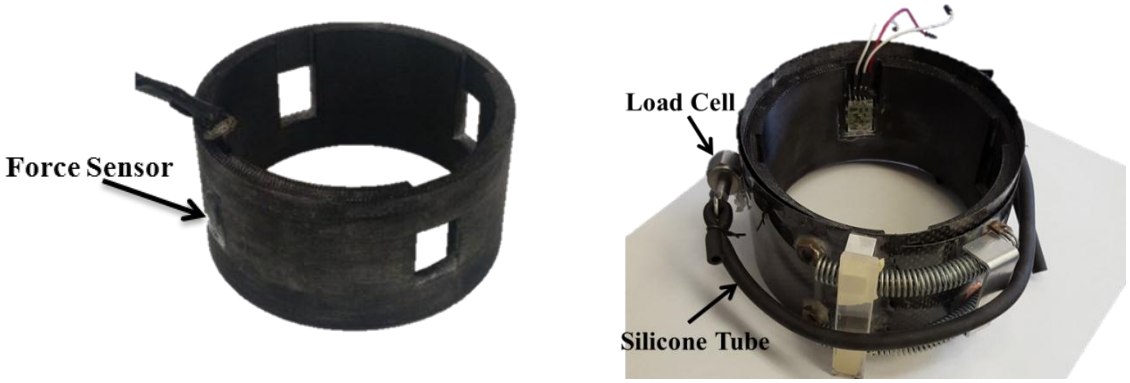

(a) **(b)**

Figure 4-2. (a) 3D printed test bed. (b) Test setup to determine relationship between applied pressure change and tension relaxation.

(a) **(b)**

Figure 4-3. Complete active compression system utilizing: (a) OBM. (b) SBM.

Figure 4-4. DE connected around test bed without belt mechanism.

4.2 Results

4.2.1 DE actuators

In the characterization of the DE actuators' free strain, multiple initial stretch ratios are considered to determine their effects on the actuators' free strain. The experimental results for the free strain of actuator A6-100R are presented in Figure 4-5. The notation SR in the legend is used to denote the initial stretch ratio. It can be seen in Figure 4-5(a) that a larger initial stretch ratio generally leads to a larger strain output at any given voltage. This is due to the incompressible nature of the dielectrics used, where a larger pre-stretch value causes the thickness of each dielectric layer of the actuator to decrease as predicted by equation (13), which in turn leads to a higher electric field being applied for

a given voltage. The applied electric fields can be calculated using equation (1), and the strain at various electric fields is plotted in Figure 4-5(b)**.** As shown in this figure, similar electric fields applied to the actuator at different initial pre-stretch ratios will result in similar strain outputs.

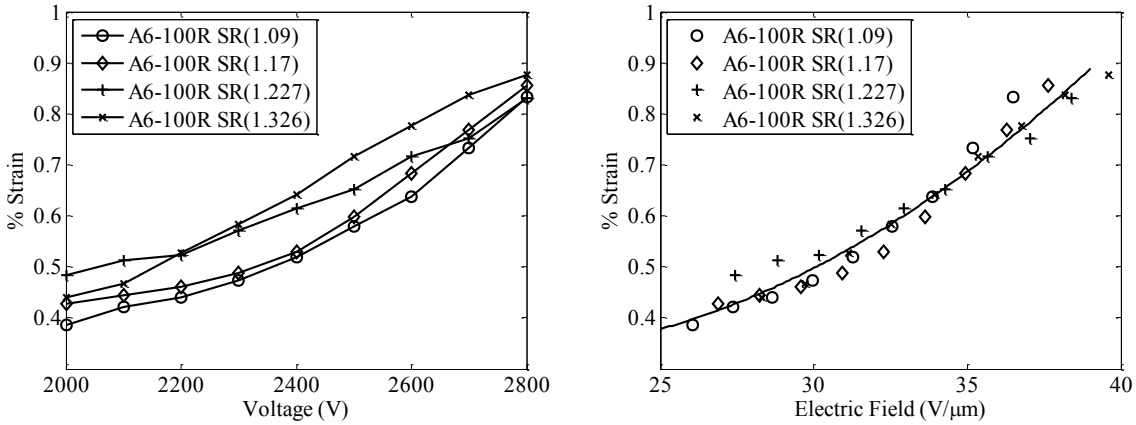

(a) **(b)**

Figure 4-5. Free strain test results for A6-100R actuator at different stretch ratios. (a) Strain vs voltage. (b) Strain vs electric field.

Figure 4-6 presents the results for the two actuators fabricated with the two dielectric materials to be compared, tested at similar stretch ratios. This is used to determine which dielectric material is capable of sustaining larger electric fields and achieving larger actuation output amplitudes. It is clear from Figure 4-6(a) that a higher strain value is achieved for the A6-50W actuator compared to the A6-100R actuator at any given voltage. The reason behind this is evident from equation (1) and is due to actuator A6-50W utilizing a dielectric material with a smaller thickness than that of the one used in the A6-100R actuator. This leads to a higher electric field being applied at similar voltages.

In order to more effectively compare between the two dielectric materials, the strain is plotted as a function of the electric field in Figure 4-6(b). The curves for the two actuators align very well due to the similar dielectric and electrode properties in both actuators. However, it is evident that actuator A6-50W can sustain significantly larger electric fields than A6-100R and thus achieves a much higher strain value of 1.7%, compared to 0.85% for A6-100R. Through this experimental testing it is shown that actuator A6-50W is capable of sustaining electric fields of greater than 50 V/μm, whereas the breakdown electric field strength of actuator A6-100R is around 40 V/μm due to imperfections in the in-lab cast silicone sheets used in the fabrication process. In addition to that, results from Gatti *et al.* [91] along with work at the University of Auckland show that the commercial silicone can be

operated safely and consistently at electric fields in excess of 60 V/μm. This is of special importance when we examine the equation for the Maxwell Pressure generated with the application of an electric field, thus leading us to expect higher strain and force values at maximum operating voltages, consistent with the analytical Maxwell Pressure curve shown in Figure 4-7 below.

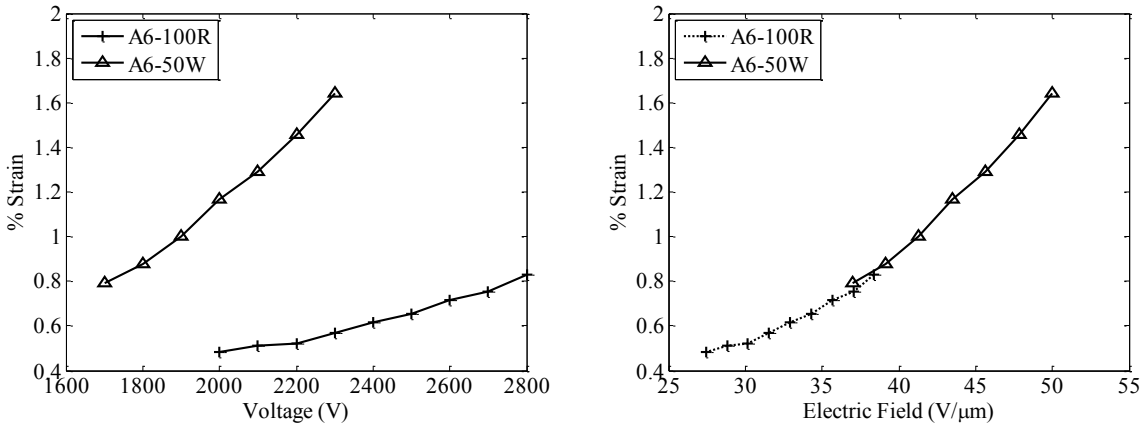

(a) **(b)**

Figure 4-6. Free strain test results for actuators A6-100R and A6-50W at similar stretch ratios. (a) Strain vs voltage. (b) Strain vs electric field.

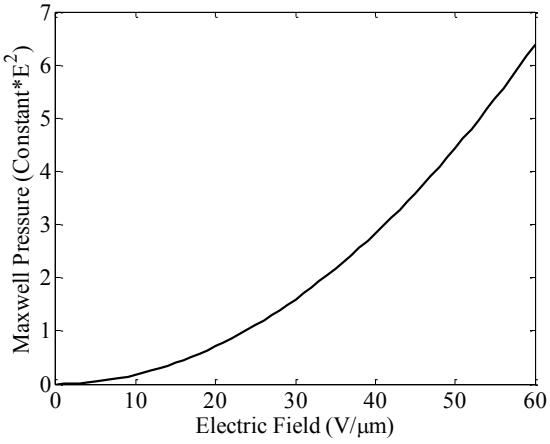

Figure 4-7. Generated Maxwell Pressure relationship to the applied electric field.

The results of a dynamic test performed in order to assess the repeatability and creep effects of cyclic actuation are presented in Figure 4-8. Actuator A6-50W is attached with an initial pre-stretch of 1.2 and is actuated cyclically at 2000 V. The actuation frequency is set at 0.2 Hz in order to provide the actuator with sufficient time to fully actuate and stabilize, thus allowing for more accurate measures

of the actuator active and inactive lengths. Experimental results indicate that an actuation induced creep of 0.15% of the length of the actuator is exhibited during the first 3.5 minutes of cyclic actuation. Following which, the actuator active and inactive lengths stabilize for the remainder of the 13 minute cyclic test. These results indicate that while creep may have non-negligible effect on the initial actuation cycles, stabilization occurs within a few minutes of cyclic testing. This information is critical to realistically assess the potential of this actuation method for cyclic active compression.

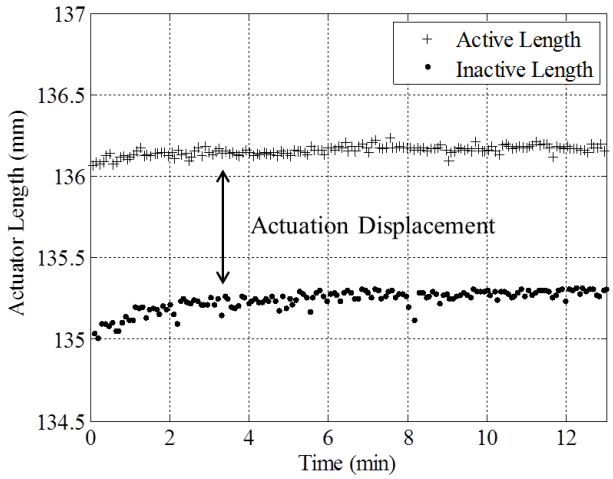

Figure 4-8. Cyclic test results for actuator A6-50W.

(a) Force-strain characterization is conducted on actuator A8-50W, with the results displayed in (b)

Figure 4-9(a). It is evident that through increasing the applied voltage, the force change to attain a given strain is reduced. This demonstrates that the active stiffness of the actuator is reduced when the applied voltage is increased. The force required to produce approximately 4.6% strain is reduced by about 8% upon applying a voltage of 1,500 V to the actuator. Additionally, blocked force testing is conducted on actuator A8-50W and the results are shown in Figure 4-9(b). A tension relaxation of 0.65 N is achieved at an applied voltage of 1500 V. The results from blocked force testing are utilized, through equation (9), in order to obtain an estimate of the expected pressure change during complete system testing.

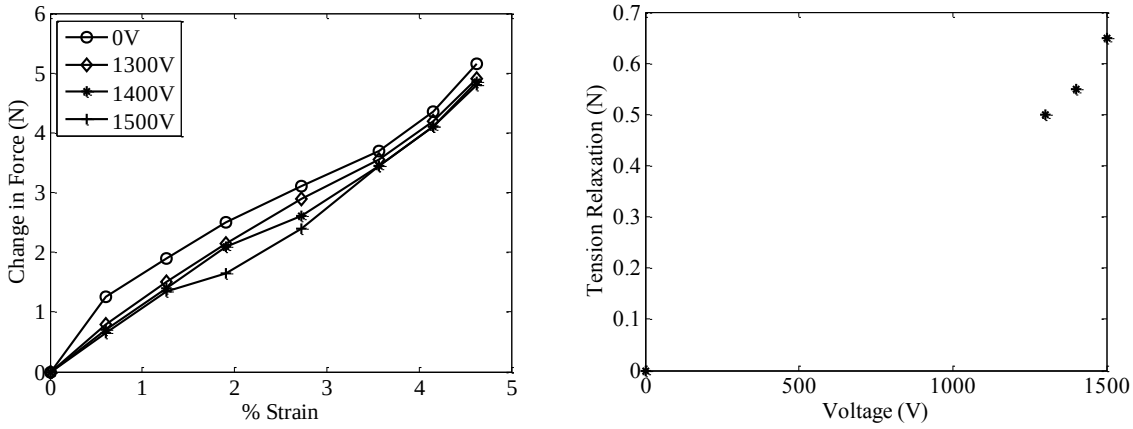

(b) **(b)**

Figure 4-9. Actuator A8-50W. (a) Force-strain testing results. (b) Blocked force testing.

The DE actuator and spring test is conducted on actuator A8-50W for two initial stretch ratios, 1.09 and 1.18, results shown in Figure 4-10. It can be observed that, as expected, the initial mechanical tension at higher stretch ratios is higher. Additionally, the tension relaxation incurred at the 1.18 stretch ratio is larger than that incurred at the 1.09 stretch ratio, at similar voltages. This is again due to the fact that at higher stretch ratios the actuator is thinner and therefore a larger Maxwell Pressure is generated.

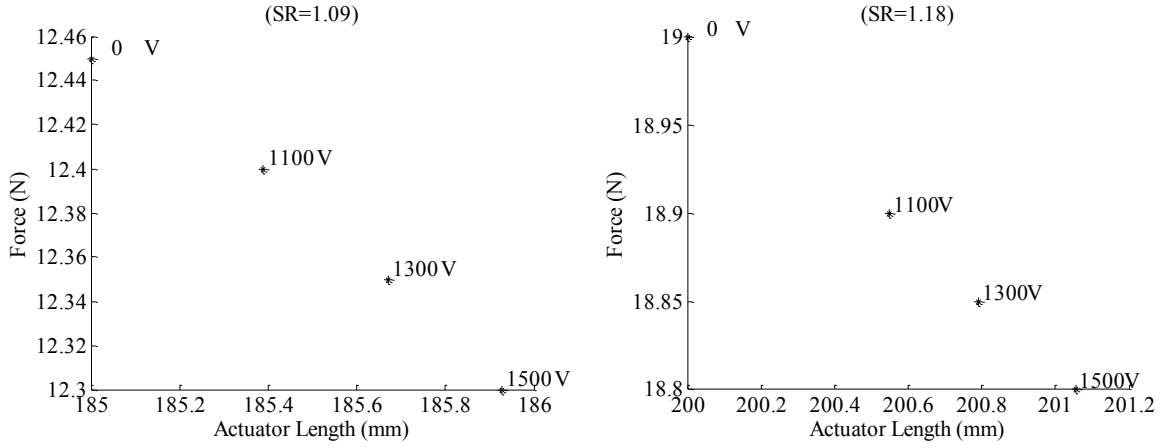

(a) **(b)**

Figure 4-10: Force vs actuator length. a) Stretch ratio 1.18. b) Stretch ratio 1.09.

4.2.2 Belt Mechanism Validation

The test setup used to validate equation (9) is shown in Figure 4-2(b). Testing is conducted with the soft belt mechanism (SBM) and the original belt mechanism (OBM). As shown in Figure 4-11(a), both the experimental and theoretical results indicate an increase in radial pressure on the core object for larger tension relaxation values. The average error between experimental and analytical results for the OBM and the SBM is about 4.3% and 6.7% respectively. Unaccounted for friction is a potential source of error during experimental testing. From the results shown, it can be deduced that for every 1 N of tension relaxation, a 3 mmHg increase in the applied radial pressure is observed.

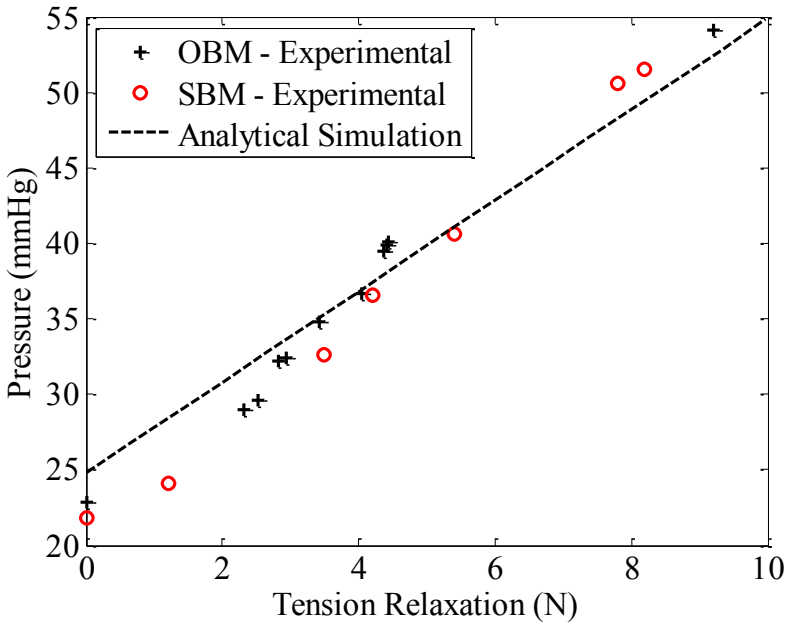

Figure 4-11. Analytical model validation: Compressive pressure w.r.t tension relaxation.

To determine uniformity of the pressure around the core object the pressure is measured by placing a piezo-resistive sensor (Interlink Electronics FSR 402) between the belt mechanism and the test bed and measuring the pressure at five points covering an overall length of 40% of its circumference. It is determined that the pressure distribution is relatively uniform with a coefficient of variation of 4.95%.

The results investigating the effects of spring free length on the initial pressure applied by the actuation system consisting of the OBM and a DE actuator are presented in Figure 4-12. Actuator A8-50 W is used in this testing at a stretch ratio of 1.28 resulting in a pre-tension, F_m, of about 19.8 N. These results are compared to the same actuator with an identical pre-stretch ratio connected without

the belt mechanism, test setup shown in Figure 4-4. An advantage of using the belt mechanism in conjunction with a DE actuator is that the pre-compression on the cuff can be tuned to smaller values despite having large stretch ratios in the actuator, due to the counteracting spring force. For the A8-50W actuator, the initial mechanical pressure can be set anywhere between 26.7 and 120.1 mmHg as shown in Figure 4-12. A larger initial pressure is expected for larger spring free lengths since they have to undergo a larger compression in order to achieve the same final length, *L*. This behavior is also observed experimentally and compares quite well to the analytical model presented by equation (15). The average percentage of difference between the experimental and analytical pressure is about 3.75%, with the maximum percentage difference of 6%. On the other hand, initial pressure applied by the actuator connected without the belt mechanism can only be varied by changing the stretch ratio or utilizing an actuator of a different stiffness.

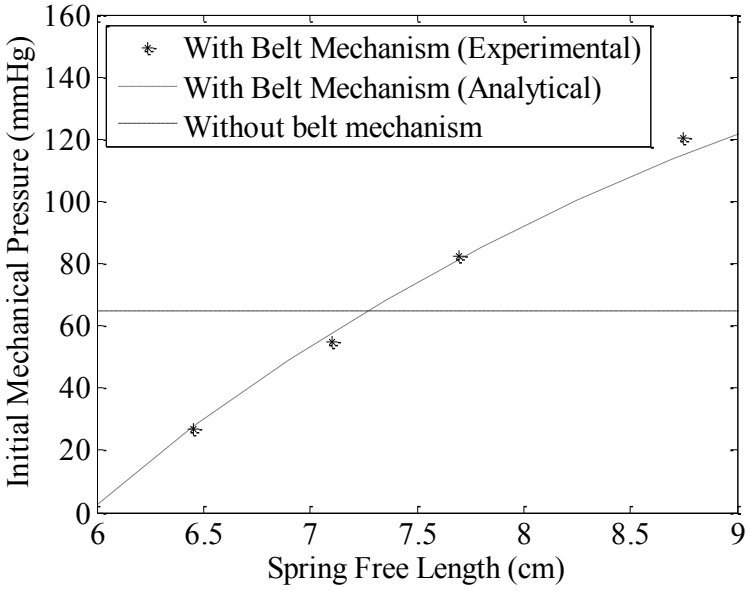

Figure 4-12. Analytical model validation: Initial pre-compression w.r.t spring free length.

4.2.3 Active Compression System Testing

Active compression testing utilizing either belt mechanism in conjunction with a DE actuator shows that as the voltage applied to the DE actuator increases, the applied pressure also increases. The pressure change with voltage application at three different initial pre-compression values, for the complete system utilizing the OBM in conjunction with actuator A8-50 with a pre-stretch of 1.25, is presented in Figure 4-13(a). The initial pre-compression is varied by utilizing springs of different free

lengths. Equation (9) anticipates that the pressure change due to the tension relaxation, F_e, should not be significantly affected by the initial pre-compression value of the belt mechanism. However, it is observed experimentally that there is a minimal increase in the pressure gradient as the initial pre-compression value is increased. This slight variance is attributed to small differences between the spring's compressed lengths among these tests, where it is assumed in the analytical formulation that the spring's compressed lengths remain constant for all the conducted tests at various initial pre-compressions.

The pressure change during actuation for the active compression sets utilizing the OBM and actuators A14-50W and A8-50W is presented in Figure 4-13(b). The actuators are connected with a pre-stretch of 1.25 and the active compression set induces an initial pre-compression value of approximately 26 mmHg. As expected, the active compression set utilizing actuator A14-50W produces a larger pressure gradient when compared to that utilizing actuator A8-50W. This is due to the fact that A14-50W possesses 6 additional active layers thus amplifying the achievable tension relaxation and in turn the systems pressure change during actuation. A pressure change 2.55 mmHg is achieved at 1200 V.

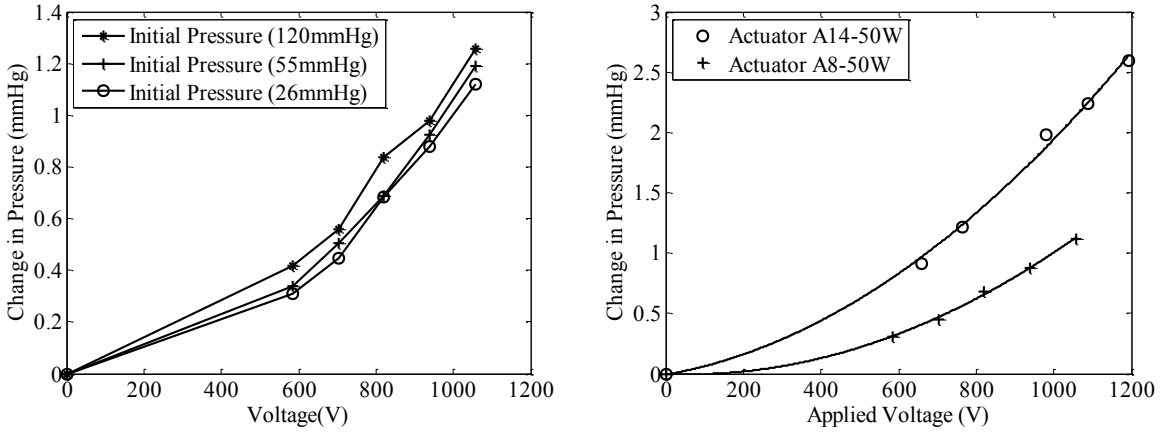

(a) **(b)**

Figure 4-13. Experimental pressure gradient with voltage application for the active compression system utilizing the OBM and: (a) Actuator A8-50 at various initial pre-compression values. (b) Actuators A14-50W and A8-50W.

The soft belt mechanism was then tested in conjunction with A14-50W as shown in Figure 4-3(b) and the results were compared to those obtained during testing with the OBM. It is shown that at low voltages the results differ more significantly, where the system with the SBM begins exhibiting a

change in pressure at a higher actuation voltage. Additionally, the pressure change at all voltages is slightly lower than that of the system utilizing the OBM This difference in results becomes less substantial as the voltage increases. Based on the experimental testing, the difference is thought to be attributed to a higher friction in the SBM due to the Kevlar fabric used in its fabrication. As the voltage is increased and in turn a larger tension relaxation is incurred, this change decreases dramatically to a 10% difference at 1200 V. The results for the experiment are shown in Figure 4-14 below. It is shown that at an actuation voltage of 2000 V, both active compression sets successfully achieve pressure gradients in excess of 5 mmHg.

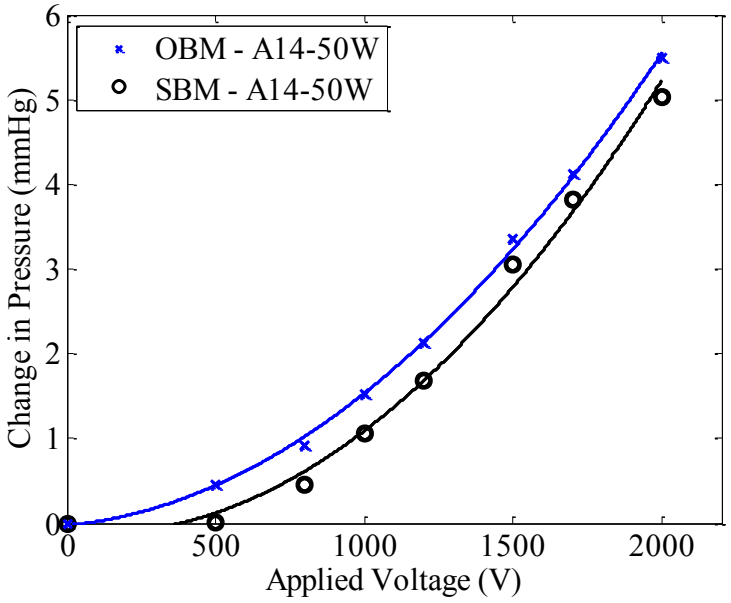

Figure 4-14: Comparison between actuation pressures using SBM and OBM.

4.2.4 Actuator Failures

This section outlines the failures experienced by two of the actuators during these tests and the possible reasons behind said failures. Actuators A12-50W and A30-50W suffered catastrophic failure immediately during testing. The failure locations in both actuators are shown in Figure 4-15.

Figure 4-15. Actuator failure locations. From left to right: A12-50W, A30-50W.

DE actuators fail for a variety of theoretically defined reasons such as dielectric strength breakdown, pull-in failure, or material strength failure. In addition, for actuators produced using manual fabrication, actuator failures can happen due to several additional localized effects such as defects introduced during the fabrication process, and mechanical stress or electric field concentrations [67]. In the case of actuator A12-50W, failure occurs due to a localized defect that is likely to have been introduced during the fabrication process. That is the case since failure occurs away from the boundary of the actuator at an electric field lower than the breakdown field strength of the dielectric material.

On the other hand, actuator A30-50W experiences catastrophic failure directly at the electrode boundary connection points. This presents a case where the applied voltage is larger than the breakdown field strength of the air gap between two of the electrodes near the boundary. This results in a spark and subsequently causes the actuator to fail. Possible causes for this are the small buffer region of 2mm on either side of the electrodes and errors in aligning the electrodes at the center of the dielectric layer. The standard breakdown field strength of air is about $3(10^6)$ V/m [92], as compared to a breakdown field strength of approximately $50(10^6)$ V/m for the dielectric material used. Therefore, at 2,000 V a spark would form if the air gap between the two conductors were less than 0.66 mm. To avoid this problem, the buffer region is doubled to a total of 4 mm at each side for subsequently fabricated actuators.

4.3 Discussion

This chapter presents the details and results of testing conducted for the static analysis of a DE based active compression set. In an effort to define the ideal system parameters and assess the effectiveness of DE actuation for an active compression application, DE characterization is conducted. Through free-strain testing, it was shown that the commercial Wacker silicone film is a more effective dielectric material than an in-lab cast RS silicone given its capability to sustain a larger electric field and in turn achieve more significant actuation amplitudes. Additionally, it was observed that the strain response of DE actuators at a given electric field is relatively unaffected by the initial stretch ratio, within a range of 1.1-1.3. Preliminary cyclic evaluation was conducted and results showed that the DE actuators exhibited minimal creep effects during the cyclic actuation and present repeatable results, thus paving a path forward to the dynamic testing presented in the coming chapter.

The presented analytical model which characterizes the belt mechanism was validated experimentally with less than 7% error for the SBM and the OBM. It was shown that compression could be applied directly with voltage application, and in turn DE expansion, through utilizing the novel active compression design. Additionally, experimental testing confirmed that the initial pre-compression exerted on the test bed before actuation could be directly controlled by changing the spring system parameters. For both proposed designs, (systems utilizing OBM and SBM), experimental and analytical results indicated that a 1 N tension relaxation in the actuator incurs approximately a 3 mmHg increase in the applied compression. Finally, in full active compression set testing, a pressure gradient of >5 mmHg was achieved through utilizing the OBM and SBM in conjunction with actuator A14-50W. It was observed that the system utilizing the SBM achieved slightly lower pressure gradients at a given voltage. However, given the significant advantages of the SBM over the OBM in terms of flexibility, breathability and light weight, the SBM remains the more effective belt mechanism and is utilized in subsequent testing.

There exist several limitations to be addressed. The voltage needed to achieve full DE actuation remains high therefore presenting safety concerns for the wearer, and necessitates additional insulation to minimize the risk of harmful electrical discharge. Through reducing the thickness of the dielectric layers, or utilizing dielectric materials with higher dielectric constants, the activation voltage can be further reduced. Additionally, actuator lifetime remains a critical issue in DE design which is not examined in this chapter.

The work presented in this chapter addresses several issues currently associated with active compression devices. Portability is achieved through utilizing a smart material based system to achieve compression, something not currently possible when utilizing non-ambulatory pneumatic compression systems. Additionally, prior published work on utilizing DE actuators for active compression has achieved pressure variations in the order of 1 mmHg while using a single layered actuator, activated at 13 kV. More importantly, due to the intrinsic operating nature of DE actuators which exhibits expansion with voltage application, compression could only be applied through maintaining an applied voltage in the relaxed state and removing the voltage in order to incur compression with actuator contraction. The system tested in this chapter was shown to be capable of applying compression directly with voltage application, thus reducing the time the actuator is charged and in turn reducing current leakage and power requirements. Furthermore, through utilizing thinner dielectric layers in a multi-layered actuator design, a 5 mmHg pressure gradient is achieved when connected in conjunction with the belt mechanism at lower voltages (1-2 kV). Presented results show that the active compression system can be set at pre-compression values similar to those used in traditional compression garments and can achieve a pressure gradient with voltage application, thus demonstrating its potential to be utilized as an active method to promote blood flow in the lower limbs. The coming chapter will examine the dynamic effectiveness of the active compression set and its constituents.

Chapter 5
Dynamic Testing

5.1 Introduction

The work presented in Chapter 3 and 4 introduced a novel smart active compression design utilizing a belt mechanism connected in conjunction with a DE actuator. This method allows the user to apply compression directly with voltage application, and maintain a given initial pre-compression value on the test bed while varying actuator dimensions, stiffness, and initial pre-stretch freely. A 5 mmHg compressive pressure increase with static voltage application was achieved.

To date, there is no published work on a cyclically operated DE based active compression system. There have been efforts, however, to characterize the frequency and dynamic response of DE actuators. A DE based tactile display device that is actuated cyclically is presented in Phung *et al.* [93] and results present a reduction of 60% in the output displacement amplitudes as the frequency of actuation is increased from relatively static at 0.1 Hz to dynamic at 10 Hz. Additionally, Molberg *et al.* [71] characterizes the strain response at different frequencies for PDMS, acrylic VHB, and thermoplastic elastomer based DE actuators. It is shown that for all tested elastomers, the output strain decreases and the loss tangent (tan δ) increases with increasing frequency. This is attributed mainly to the augmented viscous effects at higher frequencies. This hypothesis is supported by the results which show that the highly viscoelastic VHB's performance drops the most significantly at high actuation frequencies. Additional works including Palakodeti & Kessler and Fox & Goulbourne [94, 95] analyze the dynamic response of DE actuators, where the general consensus is that dynamic actuation output amplitudes are significantly lower than static or low frequency outputs, and materials that exhibit high viscoelasticity's are the most affected by this phenomenon.

There presently exists no work attempting to counteract this phenomenon and improve DE actuation output at any given frequency without attempting to alter the material properties of the elastomers. This chapter proposes and introduces a method termed the "hold time method" which is incorporated in order to increase output amplitudes during dynamic actuation through manipulating the DE input signal shape. Through utilizing this method, experimental testing will confirm that the difference between actuation output amplitudes during dynamic and static actuation can be significantly reduced. Additionally, through optimizing the parameters of the hold time method, the standardized actuation output shape with hold time implemented is almost identical to that without hold time

implemented. Therefore, there is an increase in output amplitudes with no undesirable changes in output signal shape. This methodology is analyzed and implemented on several actuators in different configurations in order to validate its effectiveness; a complete sequence of tests conducted on one actuator will be presented in this Chapter.

This chapter will begin by identifying the actuators to be tested, and introducing the hold time method. Following which, the various test beds utilized will be described in detail and the effects of dynamic actuation on actuation output magnitudes will be analyzed. The hold time method will then be characterized through its use to improve the dynamic strain and force outputs of a DE actuator and the optimal hold time parameters will be determined. Finally, the hold time method with the optimized parameters will be implemented on an active compression set in order to achieve a higher physiologically beneficial pressure gradient (>10 mmHg) during cyclic actuation.

5.2 Methods

5.2.1 Actuators

The actuators utilized for the testing in this chapter were fabricated using 50µm Wacker silicone film as the dielectric material and carbon grease as the electrode material. The various advantages and disadvantages of carbon grease electrodes and silicone elastomers are described in Section 2.3.3. Whereas the fabrication method described in Section 3.1.2.2 is utilized to fabricate the DE actuators with carbon grease electrodes. Several actuators were fabricated and tested, of which two are presented in this thesis. Actuator G2 has two active layers while actuator G28 has 28 active layers.

Actuator G2 is fabricated and tested in order to determine the influence of actuation frequency on output strain amplitudes. As shown in the prior art, the strain output is found to decrease with higher actuation frequencies. Testing on actuator G28 is performed in order to characterize the effects of the introduced hold time method in terms of achievable cyclic free strain and blocked force. Furthermore, given its large amount of active layers and in turn capability to incur significant tension relaxations with actuation, the active compression set consisting of actuator G28 connected in conjunction with the SBM is tested while utilizing the hold time method. The results of the hold time characterization are only shown for one actuator in this thesis for the purpose of succinctness. However, it is important to note that a similar hold time characterization protocol was conducted on several DE actuators, and exhibited results in line with those presented for the actuator in this thesis.

5.2.2 Input Voltage Signal Shape

The required DE actuator output shape is derived from physiological testing which provided data for lower limb active compression pulse shapes, amplitudes, and frequencies that incur a positive effect on human physiological hemodynamic response. Experimental trials showed that 400 ms compressive pulses (100 ms rise time and 300 ms fall time) applied at a frequency of 1-2 Hz incurred beneficial effects. The pulse shape was fit with sufficient accuracy to the two term Fourier Series shown in equation (16) to allow for ease of control and manipulation. The fitted curve along with the required pulse shape are shown in Figure 5-1, amplitudes are standardized to a 0-1 scale in order to effectively compare between pulse shapes. The average percent difference between the two curves is calculated to be < 10%. The curve fit is used as the input function for the actuation voltage pulses to be applied.

$$V(t) = Asin(Bt + C) + Dsin(Et + F) + G \tag{16}$$

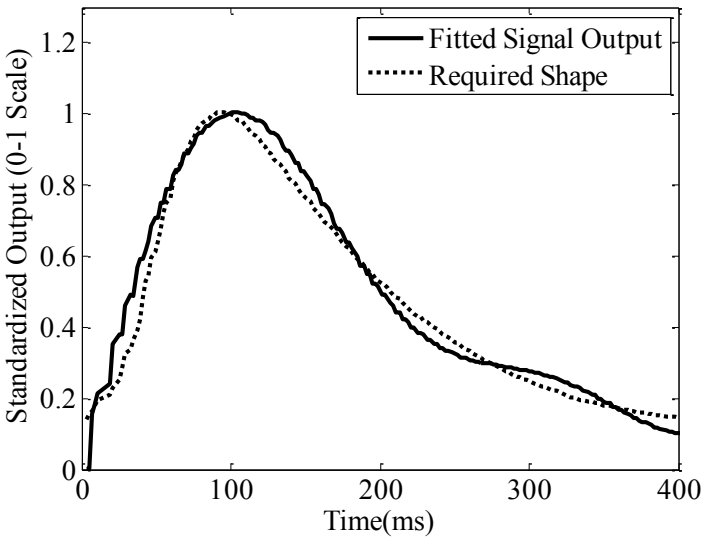

Figure 5-1. Curve fit for required output pulse shape.

5.2.3 Hold Time Method

The premise of the hold time method is to allow the DE actuators sufficient time to charge ***and*** actuate to their peak value before dropping the applied voltage. The dielectric properties of the elastomers used are not expected to vary at the frequency range in question (1-2 Hz), [71]. Therefore, the delay between the voltage peak and the actuation peak for an actuation pulse shown in Figure 5-2 appears to be entirely a function of the mechanical response time of the actuator.

At the time that the actuator has achieved its peak output, the supplied voltage has already dropped to 60% of its peak value. It is hypothesized that this reduced the maximum achievable output of the actuator. Figure 5-3(a) and (b) show the input voltage form without and with the hold time implemented respectively. It will be shown that actuating cyclically with an optimized hold time significantly increases the output magnitude while still maintaining the required actuation output pulse shape. Given the capacitive nature of the DE actuators, it is assumed that holding the voltage at a peak value for an additional fraction of a second will not incur a significant increase in power consumption, where only the current leakage must be accounted for during that short time period. Additionally, the total pulse duration does not change when implementing the hold time method.

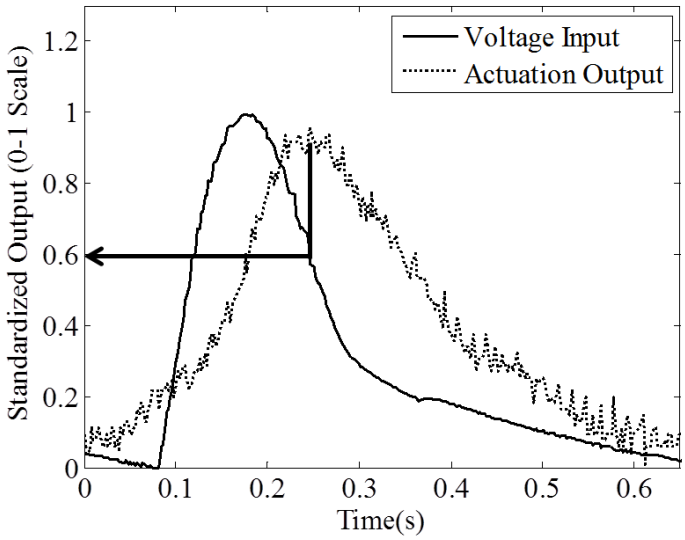

Figure 5-2. Voltage input at peak actuation output.

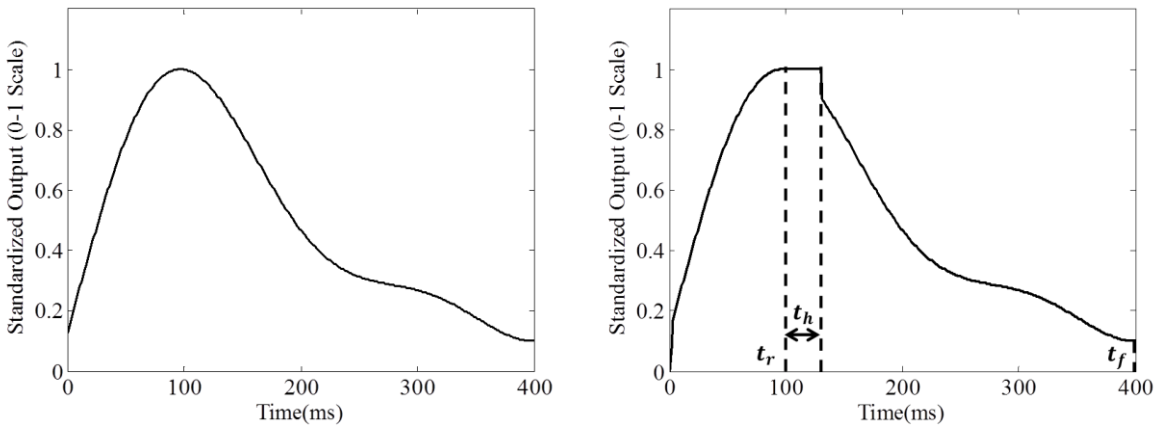

(a) **(b)**

Figure 5-3. Input voltage form. (a) Without hold time method implemented. (b) With hold time method implemented.

The equation used to control the applied voltage with hold time implemented is shown in equation (17).

$$\begin{cases} t \le t_r \ \rightarrow \ V = V(t) \\ t_r < t \le t_r + t_h \ \rightarrow \ V = V_{max} \\ t_r + t_h < t \le t_f \ \rightarrow \ V = V(t) \end{cases}$$

$$t_r = 100ms$$

$$t_f = 400ms$$

$$t_h = hold\ time \tag{17}$$

Where V(t) is the two term Fourier approximation described above, t_r is the period to reach maximum applied voltage, t_h is the time that the maximum voltage is maintained (hold time), and t_f is the total pulse duration.

The testing protocol applied in order to characterize the impact of implementing the hold time method on actuator free strain and blocked force is presented in Figure 5-4. As recommended by Carpi *et al.* [89], the actuation elongation and force are measured at every hold time after the actuator cyclic response has reached a steady state. Throughout the testing protocol, the supply voltage is kept constant while the hold time is varied.

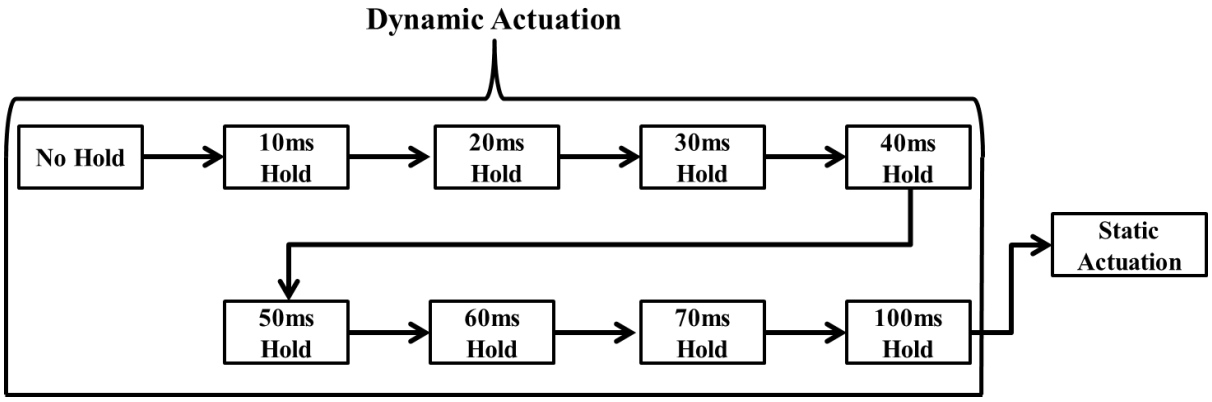

Figure 5-4. Hold time characterization testing protocol.

5.2.4 Test Setups

A series of experimental tests were conducted in order to characterize the dynamic response of the DE actuators, the effectiveness of the hold time method, and to test the active compression set cyclically. Voltage was applied using a controllable H50-PR EMCO high voltage DC-DC converter. The voltage output of the EMCO was controlled by a low voltage signal from a DAQ (NI USB-6343) using a LABVIEW control system. The DAQ is also utilized in order to acquire data from various sensors used to measure actuator elongation, tension relaxation, and applied active compression. Data is acquired at an adequate sampling rate of approximately 250 Hz. Two test setups are utilized to analyze actuator free strain and blocked force.

1) Dynamic free strain test setup (Figure 5-5): This test setup consists of hanging a DE actuator at one end and attaching a weight to the other in order to induce a pre-stretch. The ensuing actuator elongation during cyclic actuation is measured using a Keyence IL100 laser displacement sensor connected to the DAQ. In order to reduce sources of error in the acquired results due to actuator creep/stress relaxation, the actuator is provided with enough time to reach a steady state with the hanging weight before any measurements of actuation displacement are recorded, as suggested by Carpi *et al.* [89].
2) Dynamic blocked force test setup (Figure 5-6): The actuator is connected with a pre-stretch between two fixed points, one being a PCB 208C01 force sensor relaying an output signal to the DAQ. Due to the principle of operation of DE actuators, where the actuator expands with the application of a voltage, there is a measurable force change due to tension relaxation with activation.

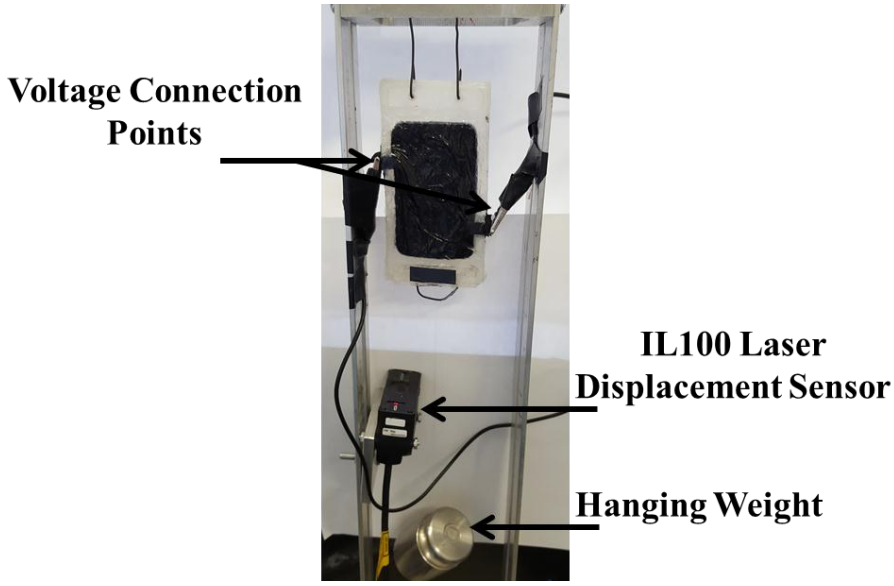

Figure 5-5. Dynamic free strain test setup.

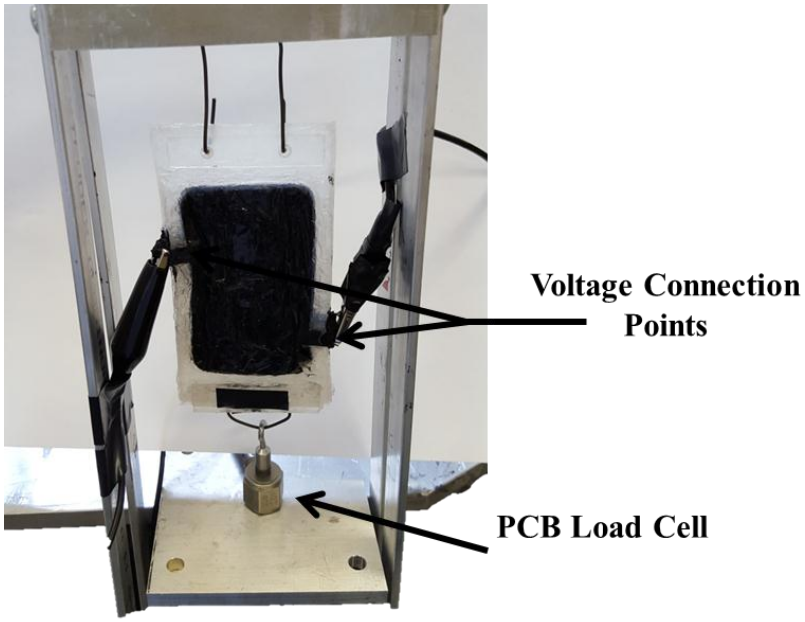

Figure 5-6. Dynamic blocked force test setup.

Active compression testing is conducted by connecting the DE actuator in conjunction with the SBM as shown in Figure 5-7. The compression system is attached around the non-deformable PCB test bed with the attached force sensor calibrated to measure applied radial pressure, described in Section 4.1.2. Through utilizing this system, active compression is applied directly with voltage application.

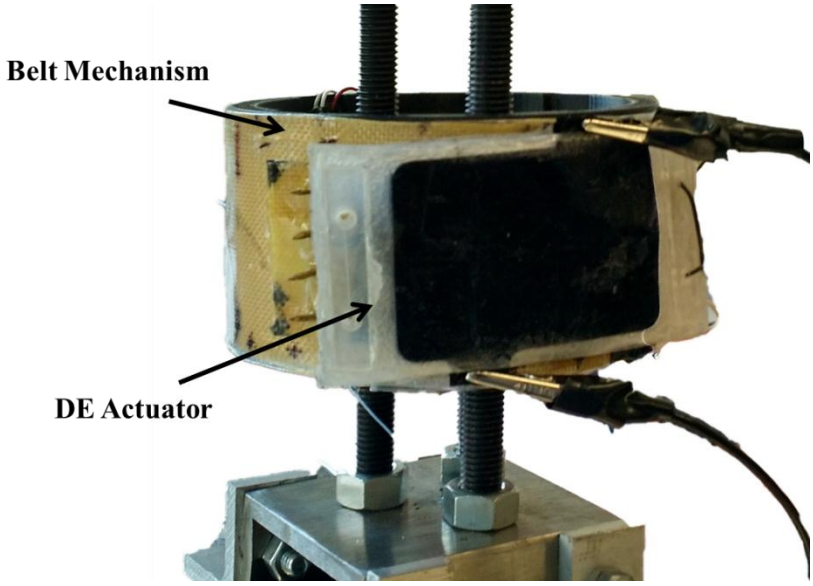

Figure 5-7. Dynamic active compression set test setup.

5.3 Results

5.3.1 DE Actuator Dynamic Testing – Hold Time Characterization

In order to characterize the dynamic response of the DE actuators, free strain testing is conducted on actuator G2 at a pre-stretch of 1.2. The frequency range to be tested for is that that is expected for normal human heartbeats (70-120 BPM), which corresponds to a 1.17-2 Hz active compression, assuming compression is applied at every heartbeat. For this purpose, the voltage input signal with amplitude of 2000 V was applied cyclically at frequencies of 1.2, 1.64, and 2 Hz, following which a static 2000 V step is applied as a baseline.

The results, presented in Figure 5-8, show that as the frequency is increased, the dynamic actuation output is reduced. At an actuation frequency of 1.64 Hz, the output strain amplitude is only 64% of that achieved during static actuation. The coefficient of variation across the three tested frequencies is less than 5%. Figure 5-9(a) shows a close-up of four voltage input pulses and the induced actuation output response. It is evident that there is a delay between the voltage peak and the corresponding output displacement peak of the DE actuator. This delay is quantified to be 70 ms and found to be constant throughout the test. Finally, it is noted that the actuation output closely follows the input voltage shape when correcting for the 70 ms delay, as shown in Figure 5-9(b). The hold time method is introduced in order to achieve a higher relative output amplitude at a given actuation frequency.

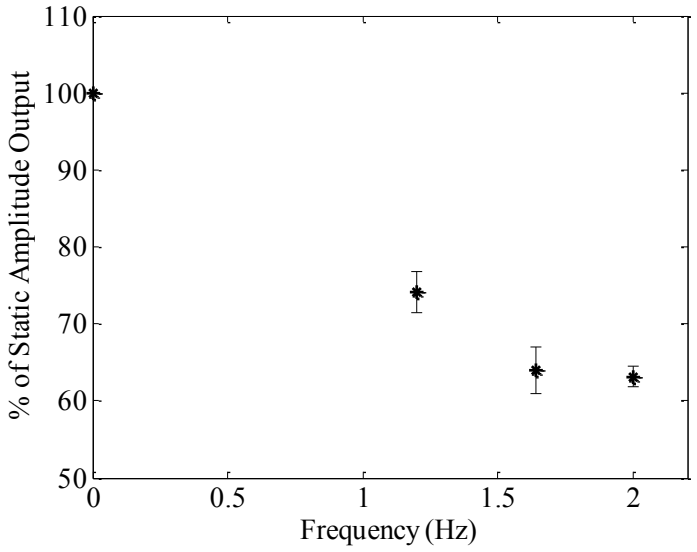

Figure 5-8. Dynamic actuation output amplitudes as percentages of static actuation output amplitude for different frequencies. Actuator G2.

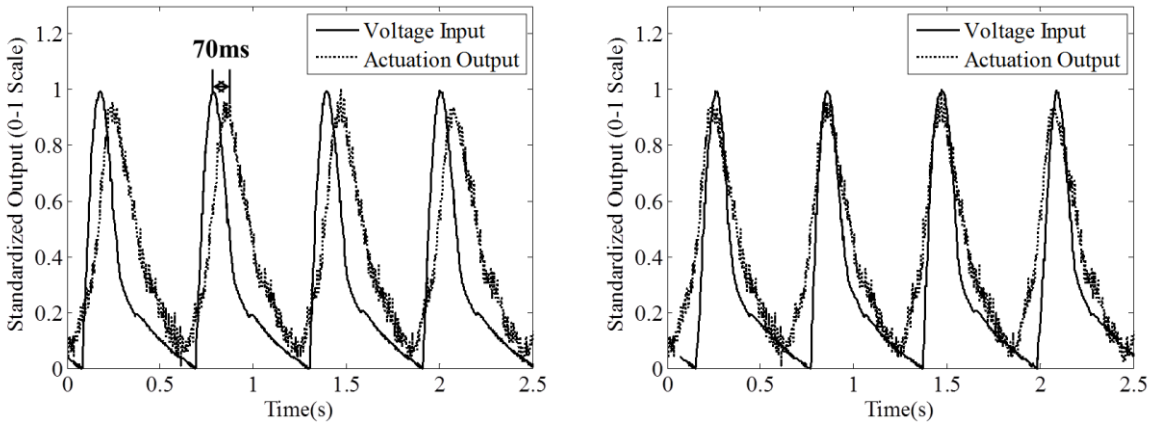

(a) **(b)**

Figure 5-9. Voltage input and actuation output pulse shapes. (a) 70ms delay shown. (b) Corrected for 70ms delay. Actuator G2.

The impacts of the hold time method are characterized through free strain testing on actuator G28 using the hold time protocol shown in Figure 5-4, at a frequency of 1.64 Hz and with a peak voltage of 2000 V. Testing is conducted for three different stretch ratios (1.06, 1.1, and 1.24) in order to determine the effect of pre-stretch on actuator dynamic response and hold time method effectiveness.

The results for the complete test for an initial stretch ratio of 1.1 are shown in Figure 5-10. It is clearly evident that at larger hold times, the actuation displacement output is amplified.

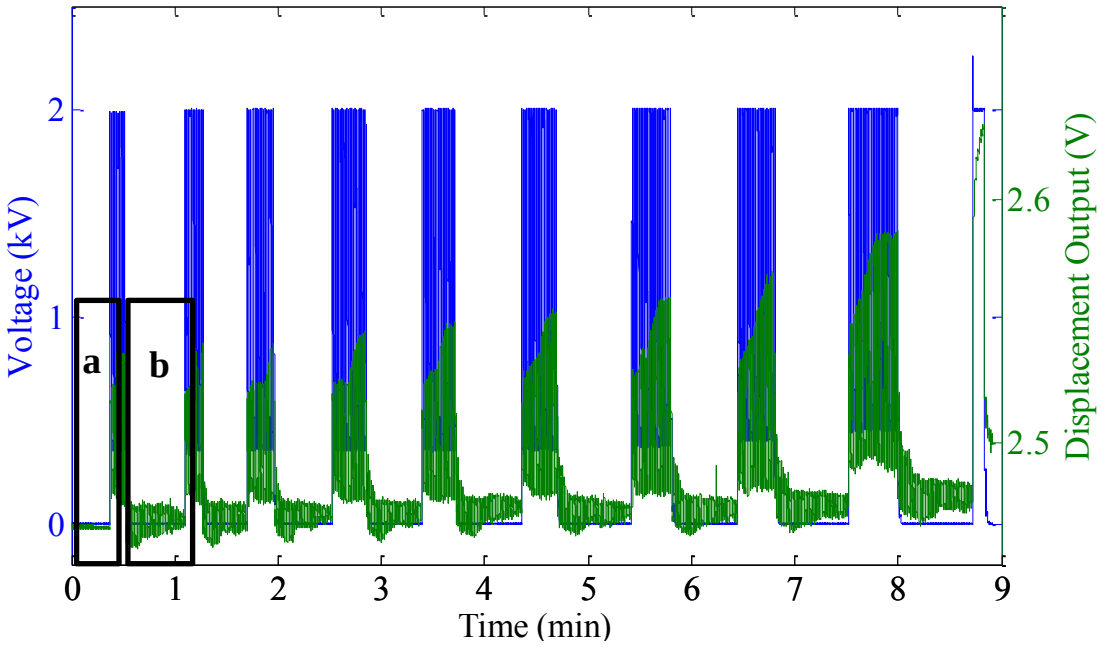

Figure 5-10: Hold time test results presenting input voltage and output strain. Actuator G28.

In order to understand the reason behind the remaining output when there is no voltage applied (see box(b) in Figure 5-10), we zoom into boxes a and b as shown in Figure 5-11 and Figure 5-12 below. Box(a) characterizes the noise of the laser displacement sensor before any voltage is applied in its equilibrium state. By zooming into box(b) as shown in Figure 5-12, it becomes clear that that the remaining fluctuation is due to the residual movement which decays over time following the removal of the voltage. This residual inertia is due to the boundary conditions of the test setup (one fixed end with other end free connected to a hanging weight).

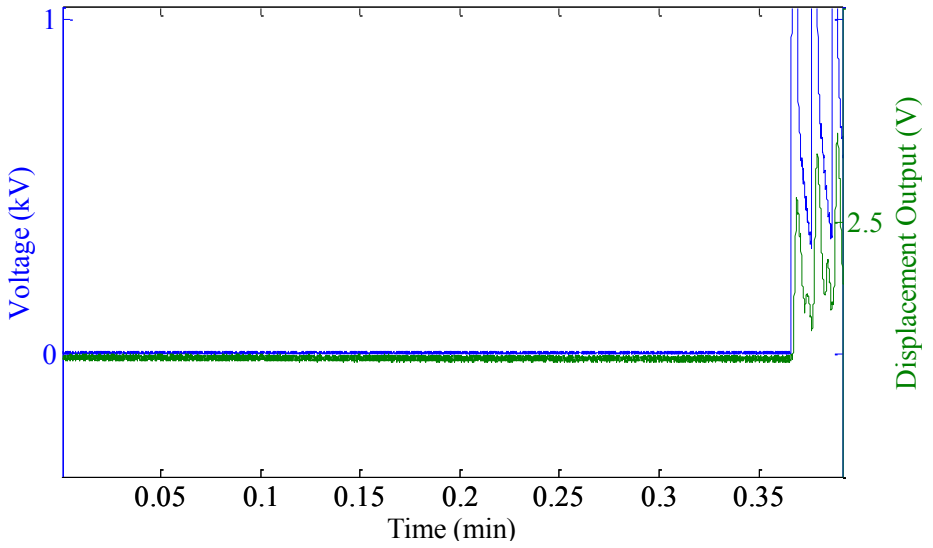

Figure 5-11: Zoom in to period before voltage application.

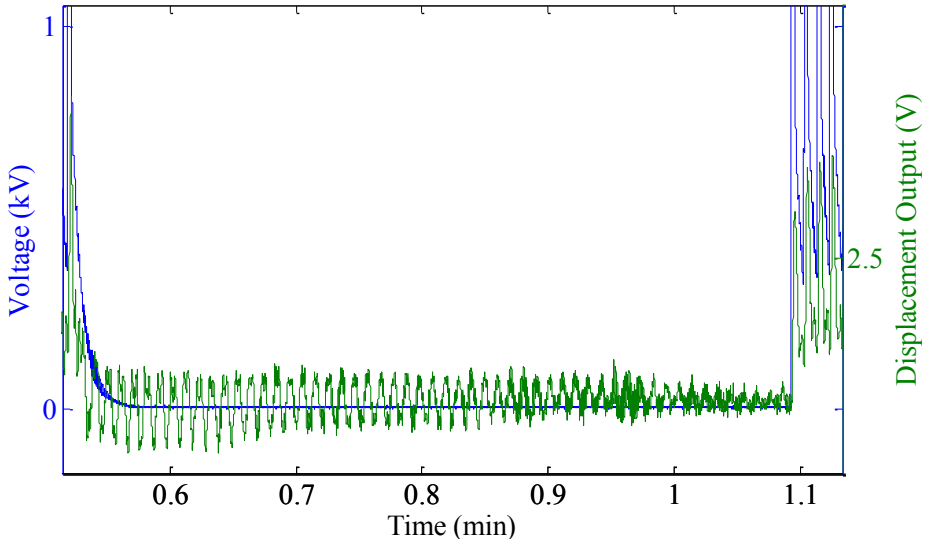

Figure 5-12: Zoom in to residual output after voltage removal.

The significant advantage of adopting the hold time method is apparent from Figure 5-13 which displays the relative output displacement at every chosen hold time as a percentage of the maximum (baseline) displacement which is achieved during static actuation. It can be seen that for a stretch ratio of 1.1, an increase from 51.4% - 77% of the baseline can be achieved through applying the hold time method. This trend is also visible for the other two stretch ratios tested, where they exhibit similar

increases in relative actuation amplitudes. Figure 5-14 is a representative plot showing the data in the previous plot in terms of a percent increase from output magnitude with no hold, due to an implementation of the hold time method. It can be shown that for the given actuator, we can achieve a 40-50% increase in output at a maximum hold time.

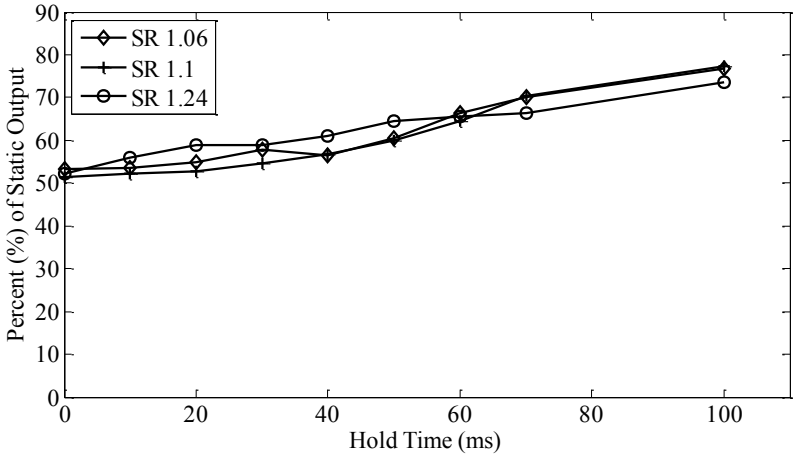

Figure 5-13. Output cyclic displacements as percentages of static displacements at various hold times for three stretch ratios. Actuator G28.

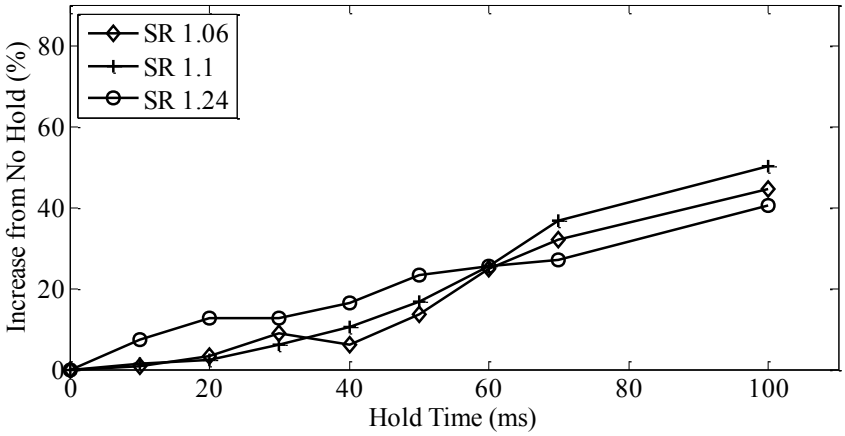

Figure 5-14. Percent increase in output magnitude due to hold time. Actuator G28.

The actuation strains at the applied pre-stretch values for the different hold times are presented in Figure 5-15(a) for actuator G28. As expected, higher strain values are observed at the higher stretch ratios, for the same applied voltage. This is due to the variances in thickness with initial pre-stretch values, where the higher the pre-stretch, the thinner the dielectric layer will be, as shown in equation

(13). Therefore, a lower thickness will lead to a higher electric field being applied by a given voltage and in turn a larger generated Maxwell stress, which is proportional to the square of the applied electric field as shown in equation (1).

Upon correcting for the initial thicknesses due to the pre-stretch ratios, and in turn the applied electric field, the corrected actuation strains are shown in Figure 5-15(b). Through examining this figure, it is observed that the initial pre-stretch value (within the tested range) is found to have an insignificant effect on actuation strain and hold time effectiveness, upon accounting for the varying thickness of the dielectric layers.

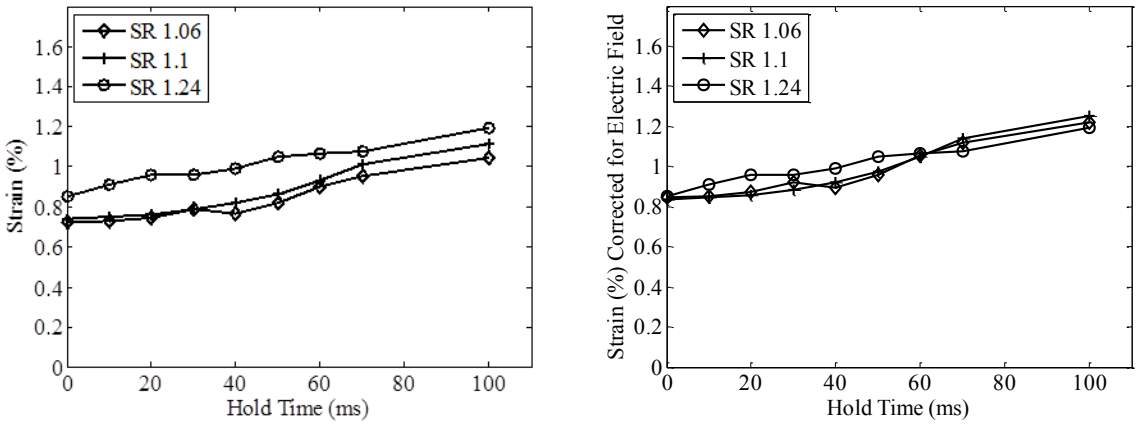

(a) **(b)**

Figure 5-15. Actuator G28. (a) strain outputs and (b) strain outputs corrected for electric field variances at different pre-stretch ratios and hold times.

The delay can be defined as the time difference between the initial voltage peak and its corresponding actuation output peak. A significant hold time delay change is defined to be one which demonstrations a greater than 15% change in delay from the no-hold time condition. The delay times for this experimental test are displayed for the various hold times and stretch ratios in Figure 5-16. The delay is determined to begin changing significantly at hold times of greater than 50 ms. This delay will be critical in determining when the undesired changes in output pulse shape due to the implemented hold time method occur, as will be shown in the coming set of results.

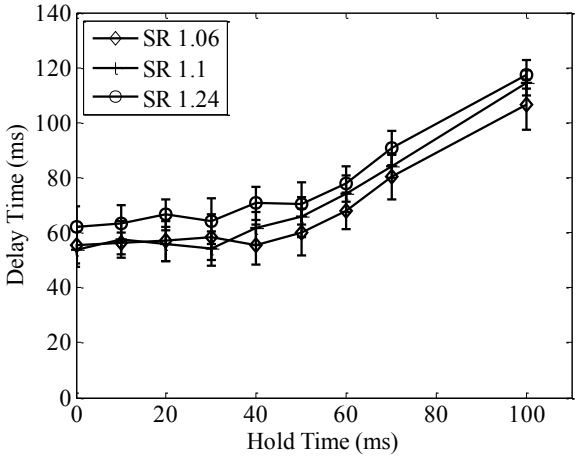

Figure 5-16. Delay times at different pre-stretch values and hold times. Actuator G28.

In order to truly determine the effects of the hold time method and to solidify its benefit/shortfall analysis, the actuator response with hold time implemented must be examined with more scrutiny. This involves inspecting actuator response at the lower lever, where the individual pulse shapes are analyzed at each hold time and compared to those obtained without the hold time method implemented. It is observed that a direct correlation is exhibited between the change in delay time and pulse shapes, where the output curve shape begins deviating from the no-hold curve shape when there is a significant change in delay time. As stated above, this is found to occur for hold times of greater than 50 ms. A comparison between the relative output magnitudes at no hold, 50 ms hold, and 100 ms hold is presented in Figure 5-17 for actuator G28 during free-strain testing with a stretch ratio of 1.24. The amplification of output magnitudes with increasing hold times is clearly observed.

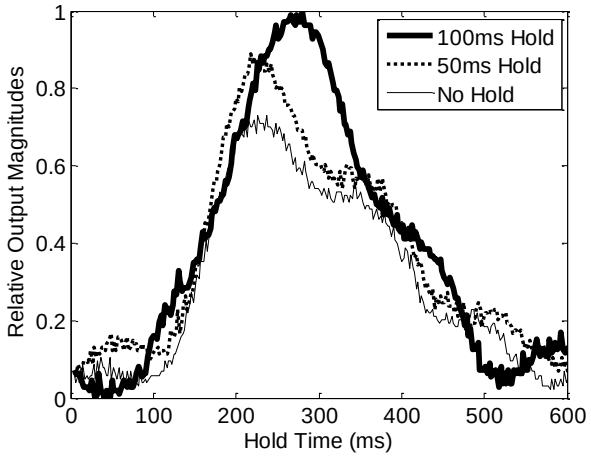

Figure 5-17. Pulse shapes at 100 ms hold, 50 ms hold, and no hold: Relative amplitudes.

The differences in output pulse shapes at the various implemented hold times can be more effectively visualized when the output curves are all normalized individually to a 0-1 scale and plotted together as shown in Figure 5-18. **It is critical to note that the plots in figure do not reflect the differences in output magnitudes.** As shown in the Figure 5-18, the curve shapes for the no hold and the 50 ms hold times show no significant differences. However, the 100 ms hold time curve presents an undesired output pulse shape where the output peak is delayed by an additional 55 ms. This corresponds with the trend of the changing delay times shown in Figure 5-16.

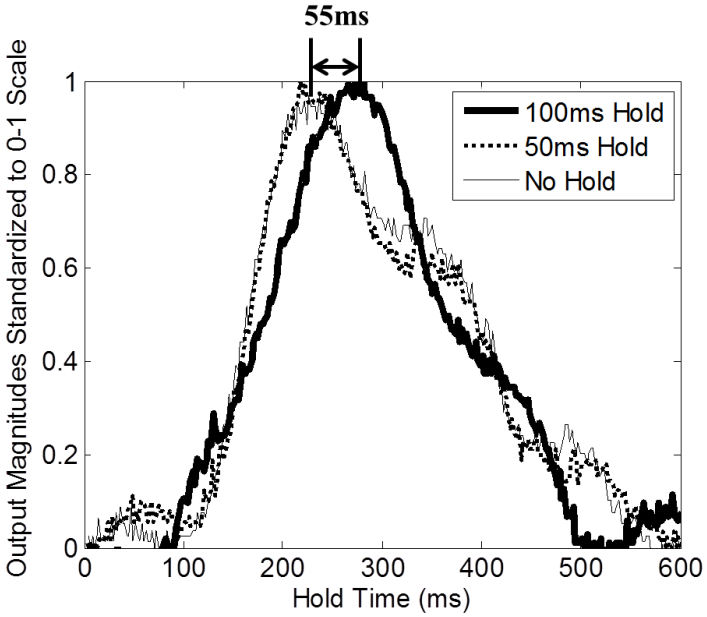

Figure 5-18. Pulse shapes at 100 ms hold, 50 ms hold, and no hold: Standardized individually to a 0-1 scale.

Cyclic blocked force testing, test setup shown in Figure 5-6, is also conducted on actuator G28 following the hold time protocol. Testing is conducted with two actuation voltages of 2500 V and 2800 V and at a frequency of 1.64 Hz. The actuator is initially connected with a pre-stretch ratio of 1.2. Figure 5-19(a) shows the induced tension relaxation during actuation at the different hold times for both applied actuation voltages. Figure 5-19(b) presents the dynamic tension relaxation as a function of the maximum tension relaxation achieved during static actuation at various hold times. Given the linear stress strain behavior of the dielectric used at this stretch ratio, the trend for the force and strain plots shown in Figure 5-19(b) and Figure 5-13 are almost identical.

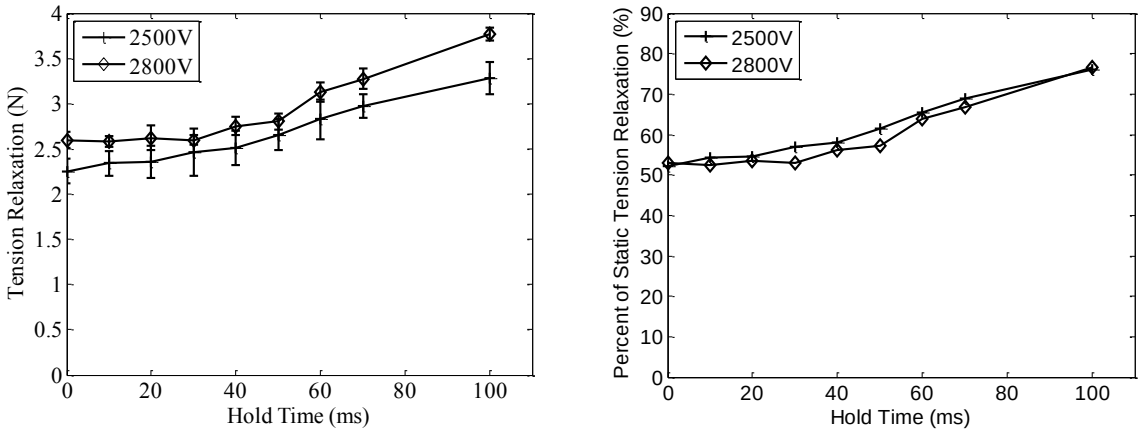

(a) **(b)**

Figure 5-19. Actuator G28. (a) Dynamic tension relaxation and (b) percent of static tension relaxation at different voltages and hold times.

Several important conclusions can be drawn from the presented results and in turn provide a basis for subsequent testing.

- Beyond a threshold hold time, increasing hold time begins inducing an increased delay time and in turn an un-ideal pulse shape.
- Implementing the hold time method leads to a larger achievable DE actuator output, where, as the hold time is increased, the actuation output amplitudes are also increased.
- An ideal hold time can be determined for any given actuator which induces a higher achievable output without affecting the output curve shape significantly; this is determined to be 50-60 ms for actuator G28.

5.3.2 Active Compression Dynamic Testing

The final set of testing utilizes the results obtained in order to achieve large pressure gradients during active compression cyclic testing. Actuator G28 is pre-stretched to a value of 1.2, thus leading to an initial mechanical pre-compression on the test bed of 22 mmHg. Actuation is applied at a frequency of 1.64 Hz with voltage amplitude of 2500 V. The dynamic active compression testing protocol involves cyclically actuating with no hold, followed by 30 ms hold, and finally 60 ms hold, and recording the incurred pressure gradients. No hold times of greater than 60 ms are utilized during active compressions testing since previous results indicated that these large hold times incur an undesired deviation from the required output shape.

Figure 5-20 presents the results for each hold time. It can be seen that the active compression set is successful in achieving a pressure change with actuation of greater than 10 mmHg, at a hold time of 60 ms. At this hold time, the actuation pressure change is increased by 30% from the no-hold output. Furthermore, the repeatability of cyclic active compression can be assessed through calculating the coefficients of variation at each hold time. These are found to be 2.4%, 3.5% and 5.5% for no hold, 30 ms hold, and 60 ms hold times respectively.

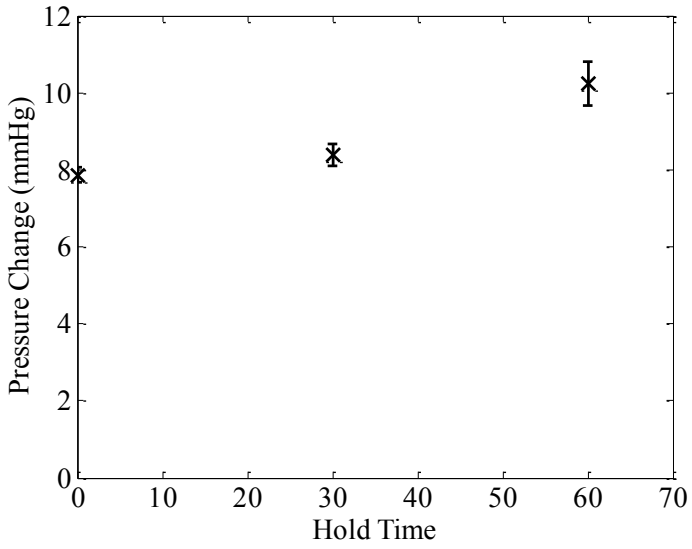

Figure 5-20. Cyclic active compression test results.

5.4 Discussion

Over the course of this chapter, the hold time method is introduced which is shown to increase dynamic actuation output amplitudes for DE actuators. This is done through manipulating the input signal shape, thus giving the DE actuator sufficient time to actuate to its peak before lowering the input voltage. This method is utilized during cyclic active compression set in order to successfully achieve the physiology mandated actuation pressure gradient of 10 mmHg.

Initially, it is demonstrated that when operating cyclically, the achievable actuation outputs are considerably lower than those obtainable during static actuation. At 1.64 Hz, actuation amplitude is only 65% of that achieved during static actuation. The effects of implementing the hold time method on actuator free strain, blocked force, and output pulse shape are characterized. Through experimental testing at 1.64 Hz, 50% and 25% increases in output amplitudes are exhibited when incorporating hold times of 100 and 60 ms respectively. Additionally it is observed that beyond a hold time threshold, increasing the hold time leads to an undesirable change in the pulse shape. Therefore, the optimal hold time of 40-60 ms is determined where there is a significant increase in output amplitudes and a negligible change in output pulse shape. Through utilizing the optimized hold time parameters, the actuator is tested in conjunction with the SBM to form the active compression set and a cyclic pressure gradient of greater than 10 mmHg is achieved.

There remain several limitations in the work presented in this chapter to be addressed in future work in this domain. Actuators in this chapter are fabricated using carbon-grease electrodes, which are not ideal for multi-layered actuators or for actuators that are required to exhibit long lifetimes. Future testing validating the effectiveness of the hold time method on actuators fabricated using different dielectric/electrode materials may prove beneficial. Additionally, similar to what is described in Chapter 4; high voltages are required to drive the DE actuator thus presenting safety concerns. Finally, while a thorough analysis of the effects hold time method on actuation outputs is presented in this work, additional work may attempt to characterize its effects on DE actuation power consumption and in turn actuation efficiency.

The work presented in this chapter builds up from that described in the previous chapter, where dynamic testing is now conducted on the system introduced and validated in Chapters 3 and 4. Through tacking an issue commonly presented in the literature and amplifying the actuation response during dynamic actuation, the active compression set achieved a physiologically beneficial actuation pressure change at a frequency of 1.64 Hz, thus proving the concept of DE based active compression.

Additionally, the hold time method, while implemented successfully for an active compression application in this study, provides the potential to improve actuation output in other applications utilizing DE actuators that may require a quick deformational cyclic pulse.

Chapter 6
Regenerative Powering System – Preliminary Analysis

6.1 Introduction

Chapters 3, 4 and 5 present the design and experimental validation of an active compression set capable of applying physiologically beneficial pressure gradients. As described previously, a complete active compression system consists of four or five active compression sets connected sequentially from the ankle to the knee as shown in Figure 2-3. These sets apply compression in series where after compression is applied at the first portion of the leg, the compression on that portion is removed as the next section is compressed, it is this staggered compression that incurs the required "milking" effect to help promote blood return to the heart.

While fabricating several active compression sets and integrating them to form an active compression system is beyond the scope of this work, a preliminary control system and circuit design that may be utilized in the future integration is presented in this chapter. This system aims to increase the power efficiency of the final system through using the energy stored in a DE actuator to charge the next actuator in the series and so forth. This reduces the amount of energy wasted as the charge in each actuator is no longer being dissipated completely as heat and instead a portion of it is being used to charge the next actuator. The work presented in this chapter will present a the design and experimental testing of a system to allow regenerative powering with two active areas, where future work could involve expanding on the design to include four or five active areas.

6.2 Preliminary Design

In order to achieve the sequential actuation of two actuators, and to save energy by charging one of the actuators with the other, the system shown in Figure 6-1 is utilized. This system is controlled by a data acquisition device (DAQ: NI USB-6343) utilizing a LABVIEW control system. The control system outputs are shown green in the diagram below, where the in-time voltage across each actuator is also acquired and recorded by the DAQ. A one layered DE actuator is modelled as a capacitor with a resistor on each face in order to account for the resistance of the electrode materials utilized. The physical regenerative powering system, shown in black in Figure 6-1, consists of a controllable high voltage power supply (EMCO H50-PR), the two actuators A_1 and A_2, and three electromagnetically actuated reed relays utilized in order to facilitate the charging and discharging of each actuator

independently and in series. The system shown in red in Figure 6-1 is utilized in order to control the reed switches; S_{w0}, S_{w1}, and S_{w2}, this is done through utilizing 3 N-CH MOSFET's (DMG1012UW-7) and a 2 ampere current source. The methods of operation of the systems are described below.

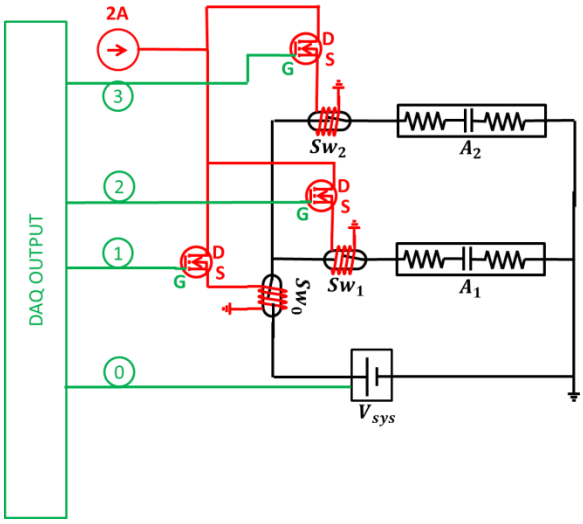

Figure 6-1: Regenerative powering system diagram.

6.2.1 Reed Relays

A reed switch is a magnetically operated electrical switch. It consists of two ferromagnetic contacts separated by a small gap, leading to an open circuit, in a hermetically sealed glass tube filled with a protective gas. Upon being in the presence of a sufficiently large magnetic field, the two contacts are magnetized and attracted to each other thus closing the circuit [96]. A reed switch which is activated electromagnetically through wrapping a coil around it is considered as a reed relay [97], this is shown in Figure 6-2(b). The reed switch utilized, (MARR-5-17-23), requires an electromagnetic field strength of 17-23 Ampere-turns (AT) to be actuated fully [98]. Therefore, through wrapping a 28 gauge copper motor wire 30 times around the reed switch and applying a current of 1A, a magneto-motive force of 30 AT is induced. The reed relay is found to be sufficiently conductive (resistance <2Ω) when fully actuated.

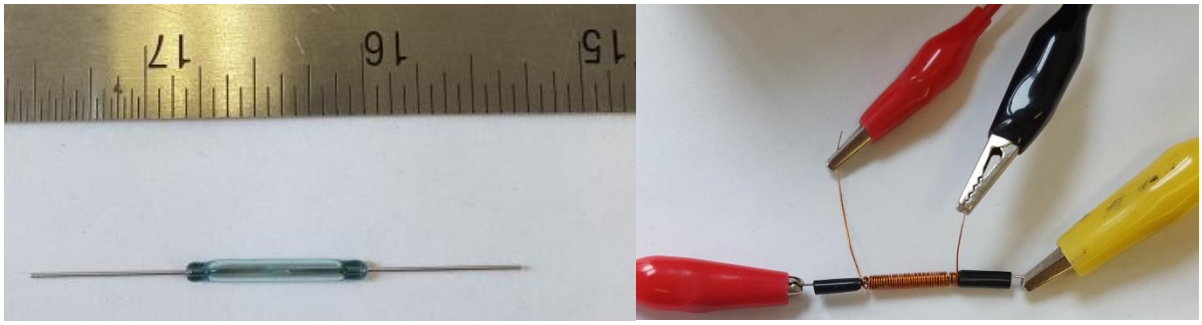

(a) **(b)**

Figure 6-2: (a) Reed switch. (b) Reed switch with copper coil wrapped around it (reed relay).

6.2.2 DAQ Outputs

As can be seen in Figure 6-1, the DAQ has four outputs utilized in order to effectively control the system. The purpose of each of the outputs is described below:

Output (0): Supply Voltage Control: A 0-5 V output signal is utilized to control the high voltage DC-DC converter which is used to charge the DE actuators.

Output (1): S_{W0} Control: A step input signal is used to control the N-CH MOSFET utilized to allow current to pass to the copper coil and in turn actuate the reed switch S_{W0}. This switch completes the circuit from the power source to the two actuators connected in parallel.

Output (2): S_{W1} Control: A step input signal is used to control the N-CH MOSFET utilized to allow current to pass to the copper coil and in turn actuate the reed switch S_{W1}. This switch completes the connection from S_{W0} to actuator A_1.

Output (3): S_{W2} Control: A step input signal is used to control the N-CH MOSFET utilized to allow current to pass to the copper coil and in turn actuate the reed switch S_{W2}. This switch completes the connection from S_{W0} to actuator A_2.

6.2.3 System Operation Protocol

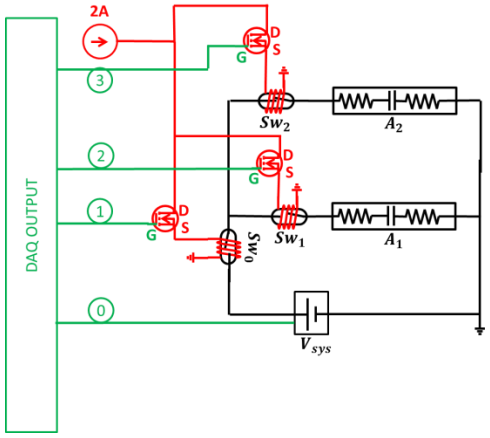

Figure 6-3: Regenerative powering system diagram.

The protocol followed in order to implement the regenerative powering system is shown below, incorporating two phases and a total of 7 steps. It is assumed that outputs (1), (2), and (3) are equal to 0 at every step if not stated otherwise.

Phase A) Charging the actuators:

1. Output (0) > 0 → V_{sys} applying voltage **
2. Outputs (1) and (2) > 0 → S_{W0} and S_{W1} closed → Charging A_1 with V_{sys}.
3. **Outputs (2) and (3) > 0 → S_{W1} and S_{W2} closed → Charging A_2 with A_1. (Regenerative Powering).**
4. Outputs (1) and (3) > 0 → S_{W0} and S_{W2} closed → Complete charging A_2 with V_{sys}.

Phase B) Discharging the actuators:

5. Output (0) = 0 → V_{sys} = 0 V **
6. Outputs (1) and (2) > 0 → S_{W0} and S_{W1} closed → Discharging A_1 with V_{sys}.
7. Outputs (1) and (3) > 0 → S_{W0} and S_{W2} closed → Discharging A_2 with V_{sys}.

***Constant for the remainder of the phase.*

The idealized theoretical actuator response case of protocol described above is shown in Figure 6-4, with the utilized timing method. It can be seen that Step 3 is where the regenerative powering occurs, it is at that point where a connection between actuators A1 and A2 is formed and the fully charged actuator A1 discharges into the uncharged actuator A2 and an equilibrium is reached at half the peak voltage. It is important to note that this is an idealized case where there is no leakage current and an

equilibrium is reached at 50% of the maximum voltage. The energy stored in a capacitor at a given voltage can be calculated using equation 18 shown below. Through examining the anticipated response in Figure 6-4 it can be determined analytically that the energy consumed to charge actuator A_2 is reduced by 25% through utilizing the regenerative powering system.

$$E_{Cap} = \frac{1}{2}\mathrm{CV}^2 \tag{18}$$

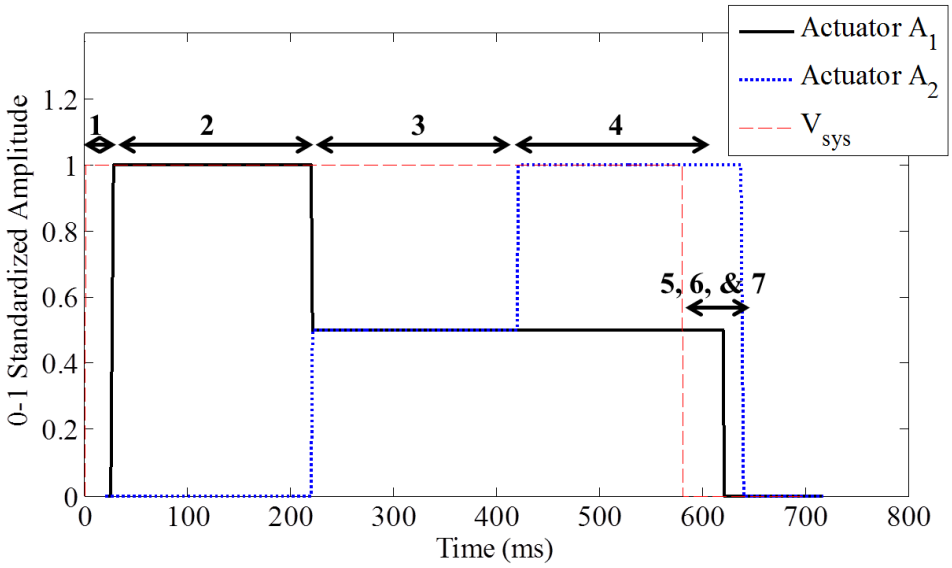

Figure 6-4: Idealized theoretical regenerative powering system response.

6.3 Preliminary Results

The first step in assessing the effectiveness of the system involved evaluating the electrical response time of the regenerative powering system, without incorporating the DE actuators. This was done through cyclically actuating the system and recording the voltage at the reed switches. Initially, before the reed relay S_{W0} is actuated, the voltage across it is the same as V_{sys} since it forms an open circuit. Upon actuating, the voltage drops to 0, as shown in Figure 6-5. It is found that the response time of the system is < 4 ms and therefore provides adequate speed to run the control timing protocol presented above.

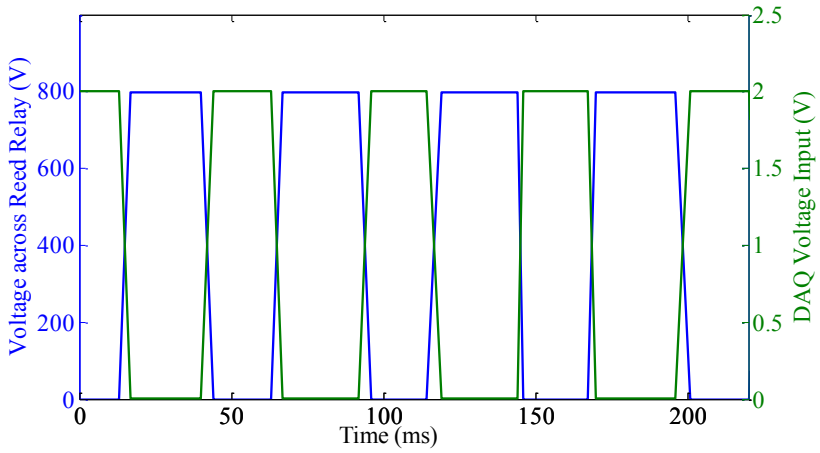

Figure 6-5: Reed relay system response time.

In order to reduce the uncertanties involved in testing the DE actuator (due to viscoelastic response of the dielectric used and electrode resistance of the carbon grease electrodes), two 330 µF capacitors are connected instead of the actuators. The results of one regenerative powering cycle is shown in Figure 6-6(a) below. It can be seen that the system operates as anticipated, where initially C1 is charged to completion from the power source, following which closed circuit is formed between C1 and C2 and they reach an equilibrium voltage of approximately 50% of the total voltage without requiring any additional energy input. Finally, C2 is charged to completion through the power source and C1 and C2 are discharged respectively. Furthermore, it is evident from Figure 6-6(a) that there are some losses during the period that one capacitor is charging the other, this current leakage is assumed to occur due to the internal resistance of the circuit components. The same test protocol is run for two 2 nF capacitors and the results are shown in Figure 6-6(b). The current leakage is more evident in this figure since capacitors with capacitances several orders of magnitudes smaller are

used, therefore a miniscule amount of charge is stored in the capacitors and the smallest current leakage will result in a significant voltage drop.

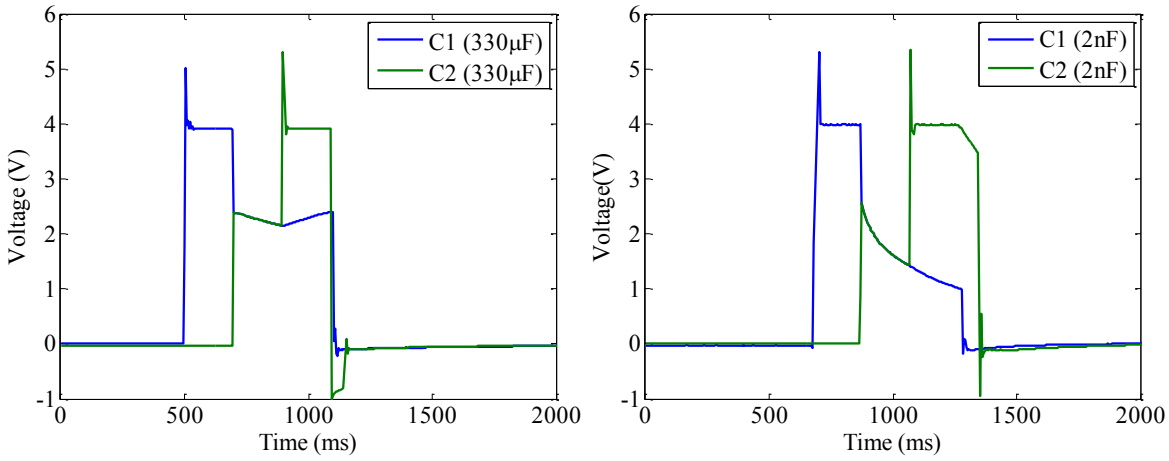

(a) **(b)**

Figure 6-6: Regenerative powering system test results incorporating two: (a) 330 μF capacitors. (b) 2 nF capacitors.

The energy consumed across three trials utilizing the 330 μF capacitors is calculated and compared to the analytical values obtained using equation (18). The following results are obtained:

1. Charging 1st capacitor from 0-4 V

Theoretical: 2.64 mJ

Experimental: 2.636 mJ (Standard deviation=0.0297 mJ)

2. Connecting two capacitors (both reach equilibrium at approximately 2 V)

Theoretical: 0 mJ

Experimental: 0 mJ

3. Fully charging 2nd capacitor from (2-4 V)

Theoretical: 1.98 mJ

Experimental: 1.976 mJ (Standard deviation=0.017711 mJ)

Therefore, experimental results show that as analytically anticipated, a total of 25% of energy is saved when charging the 2nd capacitor through utilizing the regenerative powering system. Testing is additionally conducted on the system utilizing one 0.47 µF capacitor and a one layer carbon grease based DE actuator (capacitance 2 nF), the results from this test are shown in Figure 6-7. While the system is successful in transferring charge from the capacitor to the DE actuator, we notice a significant leakage current when the actuator and capacitor circuit is formed. This is due to the resistance of the DE actuator electrodes and the resistance of the circuit components.

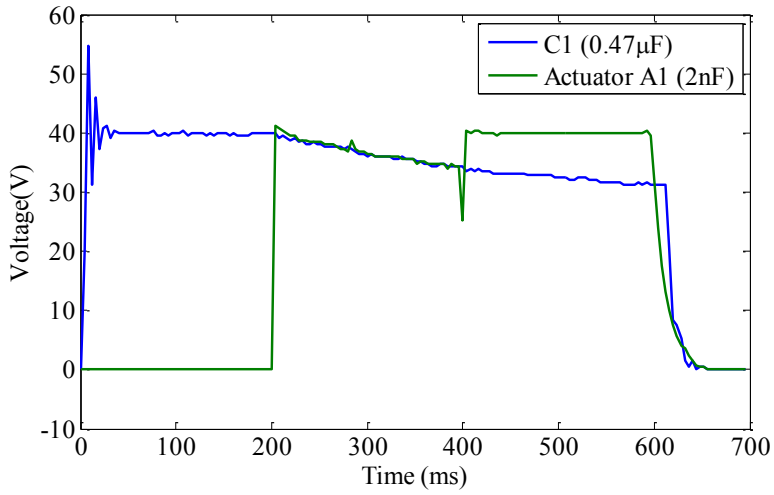

Figure 6-7: Regenerative powering system results incorporating a capacitor and a DE actuator.

Testing is finally conducted on two 2 nF actuators, where the results are shown in Figure 6-8 below. It is evident that regenerative powering does not occur when utilizing two actuators. This is due to the miniscule amount of charge stored in the actuator which is immediately dissipated as Joule losses in the high resistance electrodes of the DE actuator. Therefore, we see an initial spike in the voltage of the second actuator upon connecting both actuators together, however it is quickly dissipated and the voltage of both actuators approaches 0 V. While the system has been successfully validated for the ideal case of two low-resistance capacitors, for the current method of DE actuator fabrication utilizing relatively high resistance carbon grease electrodes, the regenerative powering system does not induce a positive energy saving.

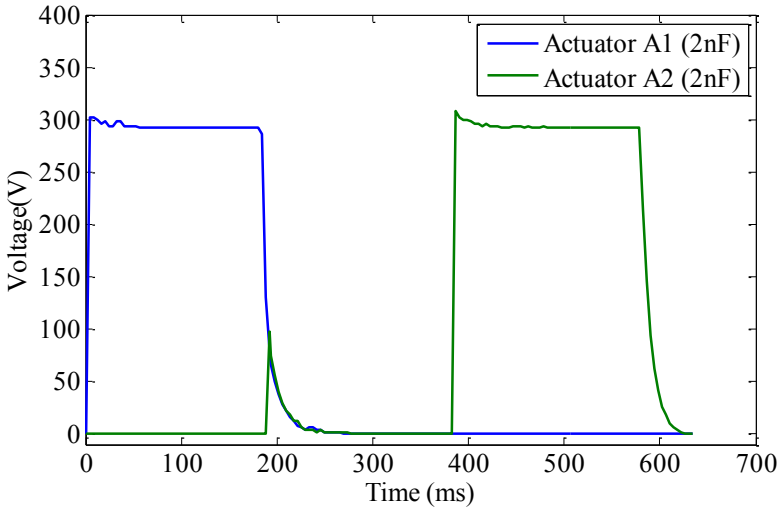

Figure 6-8: Regenerative powering system results incorporating two 2 nF DE actuators.

6.4 Discussion

This chapter presents a regenerative powering system which presents potential to be utilized to reduce energy consumption when connecting several DE based active compression sets sequentially to build a complete active compression system. Since compression is applied sequentially, thus "milking" the lower extremities, this method aims to save energy by utilizing the charge stored in one actuator to charge the next actuator in the series. This reduces the amount of wasted energy, and in turns increases the energy efficiency of the system. A regenerative powering system which aims to transfer energy across two actuators/capacitors is described in the Preliminary Design section of this chapter. Following which this system is tested utilizing two sets of low-resistance capacitors. It is found to operate effectively and successfully transfers charge from one capacitor to the other thus leading to a 25% reduction in energy consumed to charge the second capacitor.

However, upon connecting two 2 nF DE actuators with carbon grease electrodes to the system, the regenerative powering system no longer successfully transferred charge from one actuator to the other. This is due to the miniscule capacitance of the actuators and thus the small amount of charge stored within them, and the high electrode resistance. It is assumed that the charge is completely dissipated across the electrodes resistance (measured to be 25 kΩ/square using the 4-point probe method). Therefore, it is anticipated that through utilizing multi-layered actuators which incorporate electrodes with lower resistances such as nm thickness metallic or single layered carbon nanotube electrodes similar to those shown in Rosset & Shea and Yuan *et al.* [77, 83], this system can lead to

considerable energy savings as shown in the system testing incorporating the low-resistance capacitors, Figure 6-6. A major limitation of the regenerative system design presented in this chapter is that it utilizes electromagnetically actuated reed switches, which require a large amount of energy to be actuated, thus reducing the total potential energy savings of the system. This can be resolved by utilizing high voltage electronically controlled MOSFET switches therefore reducing the energy consumption and considerably simplifying the circuitry. The other limitation of this design is that the system presented only incorporates 2 actuators/capacitors, where a complete active compression system would utilize 4 active compression sets. While the principle behind the systems operation would remain the same, this would necessitate a more complex control system and circuit design.

While only preliminary analysis and testing were conducted on the regenerative powering system, it shows great potential for increasing the energy efficiency of a complete DE based active compression system. The limitations presented above, while surmountable, require future research in order to be overcome and in turn allow for the successful implementation of the system with DE actuators.

Chapter 7
Conclusion and Future Work

7.1 Conclusions

The overarching goal of this work is to develop and experimentally validate a smart active compression set. This was achieved through a novel active compression design incorporating a belt mechanism connected in conjunction a with DE actuator. This system allowed compression to be applied directly with voltage application thus reducing leakage current and strain on the actuator, therefore improving on the existing state of the art. The two constituent components of the system were thoroughly characterized and analytical equations describing the belt mechanism operation formulated and validated experimentally.

Static and dynamic testing was conducted on the system and its individual components in order to validate the active compression system effectiveness. A concept termed the hold time method is introduced during dynamic testing in order to combat the prevalent phenomenon of decreasing output actuation amplitudes at higher frequency actuation. This method was analyzed and tested on several actuators and in turn lead to an increase of 25% in output amplitudes. It was successfully implemented during dynamic testing to achieve physiologically beneficial pressure gradients during active compression. Finally, a regenerative powering circuit and control/timing system utilized to transfer charge between two capacitive components is introduced and tested.

1. *Belt mechanism allows compression to be applied directly with DE actuator expansion.*

   DE actuators actuate by expanding in area and decreasing with thickness. Therefore, the current state of the art applies compression merely with DE de-activation and shrinking. The analytical and experimental results in Chapter 4 show that the belt mechanism is successful in applying compression directly with DE actuation (expansion).

2. *Hold time method dramatically improves dynamic actuation of DE actuators.*

   The hold time method functions through manipulating the dynamic input signal to the DE actuators and in turn allowing them adequate time to charge fully before the applied voltage is reduced. This novel method was proven to experimentally increase dynamic actuator output at 1.64 Hz by 25% without any significant effect on output pulse shape.

3. *Active compression successful in attaining physiologically useful pressure gradients.*

   Through dynamic testing utilizing the hold time method in a custom powering control system, a physiologically beneficial active compression pressure gradient of > 10 mmHg is achieved at a frequency of 1.64 Hz.

4. *Regenerative powering system successful in transferring charge between two low-resistance capacitors. Ineffective for DE actuators utilizing carbon grease electrodes.*

   A DE is considered as a compliant capacitor. However, it is imperfect in that its electrodes tend to have relatively high resistances. Testing on the regenerative powering system utilizing two capacitors showed that 25% less energy was required to charge the second capacitor. On the other hand, when utilizing DE actuators, charge was not transferred and the energy requirements were not reduced. This is because the small amount of charge stored in the DE actuator was dissipated as heat across the electrodes' resistance.

5. *DE actuators are a viable option for active compression applications*

   The present state of DE actuators presents significant issues in their reliability, achievable pressures, and manufacturability. However, DE's remain a relatively young and active area of research. This work has proven that the well-rounded characteristics of DE actuators in terms achievable strains, efficiency, and actuation bandwidth can be successfully utilized in an effective active compression design.

7.2 Limitations and Future Work

While an initial leap towards achieving effective DE based active compression is presented in this thesis, there remain several limitations and in turn areas for future research in this field. The major limitations and corresponding suggestions for future work are presented below.

7.2.1 Dielectric elastomer actuators

1. *High voltage – low power requirements*

   A major limitation of DE actuators is the high actuation voltages required to achieve the Maxwell Pressures needed for significant actuation outputs. The actuators presented in this work are actuated at 1-3 kV, thus presenting safety concerns for the wearer and requiring additional insulation in order to prevent harmful electrical discharge. Additionally, the high voltage – low power requirements necessitate more complicated electronics circuits for efficient powering utilizing high voltage DC-DC converters. This remains an area of active research as shown in Huang *et al.* [99].

   In order to combat these issues, future work can fabricate multi-layered DE actuators utilizing dielectric layers with lower thicknesses or higher dielectric constants. These lower the required actuation voltage to achieve a given Maxwell Pressure, as evident in equation (1).

2. *Actuator lifetimes*

   Multi-layered DE actuators are commonly associated with short lifetimes. On the other hand some studies have shown DE actuators capable of being actuated several hundred million times without failure [62]. It is evident that the lifetime of a DE actuator is largely a function of its fabrication method and testing conditions. However, this work does not attempt to characterize the lifetime of the fabricated actuators.

   Future work performed should include fatigue tests on the actuators fabricated with different electrodes. Additionally lifetime testing should be done on the actuators when connected in the active compression system and when utilizing the hold time method. The possibility of fabricating actuators which incorporate self-healing capabilities such as those shown in Michel *et al.* and Yuan *et al.* [76, 83] should be thoroughly examined.

3. *Actuator fabrication costs*

While the raw materials utilized in DE actuators fabrication are relatively low-cost compared with other smart materials, the time and specialized equipment costs incurred due to the manufacturing process can be quite high. In this work, multi-layered DE actuators were fabricated manually in a time-intensive process in a clean room environment. This lead to a large amount of premature actuator failures and in turn wasted raw material and time. Furthermore, the equipment needed to cast carbon black-silicone electrode mixtures at the required thicknesses is costly and its absence proved to be a major limitation.

Future work should focus on setting up the infrastructure needed to fabricate multi-layered actuators more effectively, thus significantly reducing the time and material costs associated with the fabrication of a single actuator. An example of such a method is presented by Araromi *et al.* [100].

7.2.2 Regenerative powering system

1. *Regenerative powering system design*

One of the major design limitations associated with utilizing the presented regenerative powering system for an active compression system is that it is only designed to transfer charge between two capacitive elements. Additionally, the electromagnetically actuated reed relays utilized have high energy consumption thus limiting potential energy savings.

A more complex regenerative powering circuit and corresponding control system following the same principle of operation may be designed to allow the transfer of charge between five active elements. Additionally, the reed relays should be replaced with high voltage MOSFET switches, thus significantly reducing the complexity and power consumption of the circuit.

2. *Testing on DE actuators*

Results presented in Chapter 6 show that the system is not successful in transferring charge between single-layered carbon grease based DE actuators due to the small amount of charge stored in an actuator and its high electrode resistance.

It is suggested that future testing be conducted on multi-layered DE actuators with a larger active area, and in turn larger capacitance and stored charge at a given voltage. Additionally,

these DE actuators should be fabricated incorporating low resistance electrodes such as metallic or single layer carbon-nanotube electrodes.

7.2.3 Active compression system

1. *Full active compression system testing*

   This work presents the successful operation of an active compression set. However, the fabrication and testing of a complete active compression system consisting of several active compression sets connected in series is beyond the scope of the presented work.

   Future work can utilize the active compression set design in order to fabricate and test a complete active compression system.

Bibliography

[1] Pittman, R. N. (n.d.). The circulatory system and oxygen transport. Retrieved June 08, 2016, from http://www.ncbi.nlm.nih.gov/books/NBK54112

[2] Nielsen, H. V. (1982). Effect of vein pump activation upon muscle blood flow and venous pressure in the human leg. *Acta physiologica Scandinavica*,*114*(4), 481-485.

[3] Byrne, B. (2001). Deep vein thrombosis prophylaxis: the effectiveness and implications of using below-knee or thigh-length graduated compression stockings. *Heart & Lung: The Journal of Acute and Critical Care*, *30*(4), 277-284.

[4] Pedegana, L. R., Burgess, E. M., Moore, A. J., & Carpenter, M. L. (1977). Prevention of thromboembolic disease by external pneumatic compression in patients undergoing total hip arthroplasty. *Clinical orthopaedics and related research*, *128*, 190-193.

[5] Kierkegaard, A., Norgren, L., Olsson, C. G., Castenfors, J., Persson, G., & Persson, S. (1987). Incidence of Deep Vein Thrombosis in Bedridden Non-surgical Patients. *Acta Medica Scandinavica*,*222*(5), 409-414.

[6] Kahn, S. R. (1998). The clinical diagnosis of deep venous thrombosis: integrating incidence, risk factors, and symptoms and signs. *Archives of internal medicine*, *158*(21), 2315-2323.

[7] Partsch, B., & Partsch, H. (2005). Calf compression pressure required to achieve venous closure from supine to standing positions. *Journal of vascular surgery*, *42*(4), 734-738.

[8] Tochikubo, O., Ri, S., & Kura, N. (2006). Effects of pulse-synchronized massage with air cuffs on peripheral blood flow and autonomic nervous system. *Circulation Journal*, *70*(9), 1159-1163.

[9] Vanek, V. W. (1998). Meta-analysis of effectiveness of intermittent pneumatic compression devices with a comparison of thigh-high to knee-high sleeves. *The American Surgeon*, *64*(11), 1050.

[10] Morris, R. J., & Woodcock, J. P. (2010). Intermittent pneumatic compression or graduated compression stockings for deep vein thrombosis prophylaxis?: A systematic review of direct clinical comparisons. *Annals of surgery*,*251*(3), 393-396.

[11] Lao, S. B. (2016). Wearable Tactile Pressure Sensing for Compression Garments and Control of Active Compression Devices.

[12] Troynikov, O., Ashayeri, E., Burton, M., Subic, A., Alam, F., & Marteau, S. (2010). Factors influencing the effectiveness of compression garments used in sports. *Procedia Engineering*, *2*(2), 2823-2829.

[13] Wardiningsih, W., Troynikov, O., Molotnikov, A., & Estrin, Y. (2013). Influence of Protective Pad Integrated into Sport Compression Garments on their Pressure Delivery to Athlete's Lower Limbs. *Procedia Engineering*, *60*, 170-175.

[14] Ali, A., Creasy, R. H., & Edge, J. A. (2011). The effect of graduated compression stockings on running performance. *The Journal of Strength & Conditioning Research*, *25*(5), 1385-1392.

[15] Michael, J. S., Dogramaci, S. N., Steel, K. A., & Graham, K. S. (2014). What is the effect of compression garments on a balance task in female athletes?. *Gait & posture*, *39*(2), 804-809.

[16] Yu, Y. C. (2011). Mathematical Modeling of the Cardiovascular System and Its Control Mechanism. *Mathematical Physiology*, *Encyclopedia of Life Support Systems*.

[17] Cardiovascular System. (n.d.). *National Library of Medicine.* Retrieved from https://www.nlm.nih.gov/cgi/mesh/2011/MB_cgi?mode=

[18] The Cardiovascular system: The heart. (n.d.). Retreived from http://www.aw-bc.com/info/martini6e/assets/pdf/chapter21.pdf

[19] Human Anatomy. Retrieved from http://humananatomybody.info/wp-content/uploads/2015/10/Neck-Arteries-Model-Labeled-picture-yCmz.jpg

[20] Blood Flow, Blood Pressure, and Resistance. Retrieved from http://cnx.org/contents/FPtK1zmh@6.27:A4QcTJ6a@3/Blood-Flow-Blood-Pressure-and-

[21] Sheriff, D. D., Rowell, L. B., & Scher, A. M. (1993). Is rapid rise in vascular conductance at onset of dynamic exercise due to muscle pump?. *American Journal of Physiology-Heart and Circulatory Physiology*, *265*(4), H1227-H1234.

[22] Tschakovsky, M. E., Shoemaker, J. K., & Hughson, R. L. (1996). Vasodilation and muscle pump contribution to immediate exercise hyperemia. *American Journal of Physiology-Heart and Circulatory Physiology*, *271*(4), H1697-H1701.

[23] Gibbs, N. M. (1957). Venous thrombosis of the lower limbs with particular reference to bed-rest. *British Journal of Surgery*, *45*(191), 209-236.

[24] Blum, A., & Roche, E. (2005). Endovascular management of acute deep vein thrombosis. *The American journal of medicine*, *118*(8), 31-36.

[25] Lord, R. S., & Hamilton, D. (2004). Graduated compression stockings (20− 30 mmHG) do not compress leg veins in the standing position. *ANZ journal of surgery*, *74*(7), 581-585.

[26] MacRae, M. B. A., Cotter, J. D., & Laing, R. M. (2011). Compression garments and exercise. *Sports medicine*, *41*(10), 815-843.

[27] Morris, R. J., & Woodcock, J. P. (2004). Evidence-based compression: prevention of stasis and deep vein thrombosis. *Annals of surgery*, *239*(2), 162-171.

[28] Partsch, H. (2005). Compression therapy in venous leg ulcers. *Leg ulcers diagnosis and management. London: Hodder Education*, 109-16.

[29] Scurr, J. H., Machin, S. J., Bailey-King, S., Mackie, I. J., McDonald, S., & Smith, P. D. C. (2001). Frequency and prevention of symptomless deep-vein thrombosis in long-haul flights: a randomised trial. *The Lancet*, *357*(9267), 1485-1489.

[30] Belcaro, G., Geroulakos, G., Nicolaides, A. N., Myers, K. A., & Winford, M. (2001). Venous thromboembolism from air travel the LONFLIT study.*Angiology*, *52*(6), 369-374.

[31] Book, J., Prince, C. N., Villar, R., Hughson, R. L., & Peterson, S. D. (2016). Investigating the impact of passive external lower limb compression on central and peripheral hemodynamics during exercise. *European journal of applied physiology*, *116*(4), 717-727.

[32] Calne, S., & Moffatt, C. (2003). Understanding compression therapy.*Position Document of the EWMA Medical Education Partnership LTD*.

[33] Lurie, F., Scott, V., Yoon, H. C., & Kistner, R. L. (2008). On the mechanism of action of pneumatic compression devices: combined magnetic resonance imaging and duplex ultrasound investigation. *Journal of vascular surgery*,*48*(4), 1000-1006.

[34] Proctor, M. C., Greenfield, L. J., Wakefield, T. W., & Zajkowski, P. J. (2001). A clinical comparison of pneumatic compression devices: the basis for selection. *Journal of vascular surgery*, *34*(3), 459-464.

[35] Keith, S. L., McLaughlin, D. J., Anderson, F. A., Cardullo, P. A., Jones, C. E., Rohrer, M. J., & Cutler, B. S. (1992). Do graduated compression stockings and pneumatic boots have an

additive effect on the peak velocity of venous blood flow?. *Archives of Surgery*, *127*(6), 727-730.

[36] Flam, E., Berry, S., Coyle, A., Dardik, H., & Raab, L. (1996). Blood-flow augmentation of intermittent pneumatic compression systems used for the prevention of deep vein thrombosis prior to surgery. *The American journal of surgery*, *171*(3), 312-315.

[37] Malone, M. D., Cisek, P. L., Comerota, A. J., Holland, B., & Eid, I. G. (1999). High-pressure, rapid-inflation pneumatic compression improves venous hemodynamics in healthy volunteers and patients who are post-thrombotic. *Journal of vascular surgery*, *29*(4), 593-599.

[38] Leo, D. J. (2007). *Engineering analysis of smart material systems*. John Wiley & Sons.

[39] Otsuka, K., & Wayman, C. M. (1999). *Shape memory materials*. Cambridge university press.

[40] Safari, A., & Akdogan, E. K. (2008). *Piezoelectric and acoustic materials for transducer applications*. Springer Science & Business Media.

[41] Uchino, K. (1996). *Piezoelectric actuators and ultrasonic motors* (Vol. 1). Springer Science & Business Media.

[42] Kim, H. J., Koo, K., Lee, S. Q., Park, K. H., & Kim, J. (2009). High performance piezoelectric microspeakers and thin speaker array system.*ETRI journal*, *31*(6), 680-687.

[43] Koc, B., Cagatay, S., & Uchino, K. (2002). A piezoelectric motor using two orthogonal bending modes of a hollow cylinder. *IEEE transactions on ultrasonics, ferroelectrics, and frequency control*, *49*(4), 495-500.

[44] Le Letty, R., Barillot, F., Lhermet, N., Claeyssen, F., Yorck, M., Izquierdo, J. G., & Arends, H. (2001). The scanning mechanism for ROSETTA/MIDAS: from an engineering model to the flight model. *EUROPEAN SPACE AGENCY-PUBLICATIONS-ESA SP*, *480*, 75-82.

[45] Jani, J. M., Leary, M., Subic, A., & Gibson, M. A. (2014). A review of shape memory alloy research, applications and opportunities. *Materials & Design*,*56*, 1078-1113.

[46] Kohl, M. (2013). *Shape memory microactuators*. Springer Science & Business Media.

[47] Winzek, B., Schmitz, S., Rumpf, H., Sterzl, T., Hassdorf, R., Thienhaus, S., ... & Quandt, E. (2004). Recent developments in shape memory thin film technology. *Materials Science and Engineering: A*, *378*(1), 40-46.

[48] Qiu, J., Tani, J., Osanai, D., & Urushiyama, Y. (2001, March). High-speed actuation of shape memory alloy. In *Smart Materials and MEMS* (pp. 188-197). International Society for Optics and Photonics.

[49] Dynalloy, I. (2011). Technical characteristics of flexinol actuator wires. *CA: Tustin*.

[50] Jackson, C. M., Wagner, H. M., & Wasilewski, R. J. (1972). 55-Nitinol-The Alloy with a Memory: It's Physical Metallurgy Properties, and Applications. NASA SP-5110. *NASA Special Publication*, *5110*.

[51] Van Humbeeck, J. (1999). Non-medical applications of shape memory alloys. *Materials Science and Engineering: A*, *273*, 134-148.

[52] Moein, H., & Menon, C. (2014). An active compression bandage based on shape memory alloys: a preliminary investigation. *Biomedical engineering online*, *13*(1), 1.

[53] Holschuh, B., Obropta, E., & Newman, D. (2015). Low spring index NiTi coil actuators for use in active compression garments. *IEEE/ASME Transactions on Mechatronics*, *20*(3), 1264-1277.

[54] Holschuh, B. T., & Newman, D. J. (2016). Morphing Compression Garments for Space Medicine and Extravehicular Activity Using Active Materials.*Aerospace medicine and human performance*, *87*(2), 84-92.

[55] Madsen, F. B., Daugaard, A. E., Hvilsted, S., & Skov, A. L. (2016). The Current State of Silicone-Based Dielectric Elastomer Transducers.*Macromolecular rapid communications*.

[56] Bar-Cohen, Y. (2000). Electroactive polymers as artificial muscles-capabilities, potentials and challenges. *Handbook on biomimetics*, *8*.

[57] Pelrine, R., Kornbluh, R. D., Pei, Q., Stanford, S., Oh, S., Eckerle, J., ... & Meijer, K. (2002, July). Dielectric elastomer artificial muscle actuators: toward biomimetic motion. In *SPIE's 9th Annual International Symposium on Smart Structures and Materials* (pp. 126-137). International Society for Optics and Photonics.

[58] Kofod, G., & Sommer-Larsen, P. (2005). Silicone dielectric elastomer actuators: Finite-elasticity model of actuation. *Sensors and Actuators A: Physical*, *122*(2), 273-283.

[59] Carpi, F., Chiarelli, P., Mazzoldi, A., & De Rossi, D. (2003). Electromechanical characterisation of dielectric elastomer planar actuators: comparative evaluation of different electrode materials and different counterloads. *Sensors and Actuators A: Physical*, *107*(1), 85-95.

[60] Goulbourne, N., Frecker, M. I., Mockensturm, E. M., & Snyder, A. J. (2003, July). Modeling of a dielectric elastomer diaphragm for a prosthetic blood pump. In *Smart structures and Materials* (pp. 319-331). International Society for Optics and Photonics.

[61] Goulbourne, N. C., Frecker, M. I., & Mockensturm, E. (2004, July). Electro-elastic modeling of a dielectric elastomer diaphragm for a prosthetic blood pump. In *Smart Structures and Materials* (pp. 122-133). International Society for Optics and Photonics.

[62] Maffli, L., Rosset, S., Ghilardi, M., Carpi, F., & Shea, H. (2015). Ultrafast All-Polymer Electrically Tunable Silicone Lenses. *Advanced Functional Materials*, *25*(11), 1656-1665.

[63] Vogan, J. D. (2004). *Development of dielectric elastomer actuators for MRI devices* (Doctoral dissertation, Massachusetts Institute of Technology).

[64] Chakraborti, P., Toprakci, H. K., Yang, P., Di Spigna, N., Franzon, P., & Ghosh, T. (2012). A compact dielectric elastomer tubular actuator for refreshable Braille displays. *Sensors and Actuators A: Physical*, *179*, 151-157.

[65] Pei, Q., Pelrine, R., Stanford, S., Kornbluh, R., & Rosenthal, M. (2003). Electroelastomer rolls and their application for biomimetic walking robots.*Synthetic Metals*, *135*, 129-131.

[66] Plante, J. S. (2006). *Dielectric elastomer actuators for binary robotics and mechatronics* (Doctoral dissertation, Massachusetts Institute of Technology).

[67] Plante, J. S., & Dubowsky, S. (2006). Large-scale failure modes of dielectric elastomer actuators. *International journal of solids and structures*, *43*(25), 7727-7751.

[68] Kornbluh, R. D., Pelrine, R., Pei, Q., Heydt, R., Stanford, S., Oh, S., & Eckerle, J. (2002, July). Electroelastomers: applications of dielectric elastomer transducers for actuation, generation, and smart structures. In*SPIE's 9th Annual International Symposium on Smart Structures and Materials* (pp. 254-270). International Society for Optics and Photonics.

[69] Zhang, R., Kunz, A., Lochmatter, P., & Kovacs, G. (2006, March). Dielectric elastomer spring roll actuators for a portable force feedback device. In *2006 14th Symposium on Haptic Interfaces for Virtual Environment and Teleoperator Systems* (pp. 347-353). IEEE.

[70] Carpi, F., Migliore, A., Serra, G., & De Rossi, D. (2005). Helical dielectric elastomer actuators. *Smart Materials and Structures*, *14*(6), 1210.

[71] Molberg, M., Leterrier, Y., Plummer, C. J., Walder, C., Löwe, C., Opris, D. M., ... & Månson, J. A. E. (2009). Frequency dependent dielectric and mechanical behavior of elastomers for actuator applications. *Journal of Applied Physics*, *106*(5), 054112.

[72] Zakaria, S., Yu, L., Kofod, G., & Skov, A. L. (2015). The influence of static pre-stretching on the mechanical ageing of filled silicone rubbers for dielectric elastomer applications. *Materials Today Communications*, *4*, 204-213.

[73] Pelrine, R., Kornbluh, R., Joseph, J., Heydt, R., Pei, Q., & Chiba, S. (2000). High-field deformation of elastomeric dielectrics for actuators. *Materials Science and Engineering: C*, *11*(2), 89-100.

[74] Brochu, P., & Pei, Q. (2010). Advances in dielectric elastomers for actuators and artificial muscles. *Macromolecular rapid communications*, *31*(1), 10-36.

[75] Pelrine, R. E., Kornbluh, R. D., & Joseph, J. P. (1998). Electrostriction of polymer dielectrics with compliant electrodes as a means of actuation.*Sensors and Actuators A: Physical*, *64*(1), 77-85.

[76] Michel, S., Chu, B. T., Grimm, S., Nüesch, F. A., Borgschulte, A., & Opris, D. M. (2012). Self-healing electrodes for dielectric elastomer actuators.*Journal of Materials Chemistry*, *22*(38), 20736-20741.

[77] Rosset, S., & Shea, H. R. (2013). Flexible and stretchable electrodes for dielectric elastomer actuators. *Applied Physics A*, *110*(2), 281-307.

[78] Kornbluh, R. D., Pelrine, R., Joseph, J., Heydt, R., Pei, Q., & Chiba, S. (1999, May). High-field electrostriction of elastomeric polymer dielectrics for actuation. In *1999 Symposium on Smart Structures and Materials* (pp. 149-161). International Society for Optics and Photonics.

[79] Carpi, F., Salaris, C., & De Rossi, D. (2007). Folded dielectric elastomer actuators. *Smart Materials and Structures*, *16*(2), S300.

[80] Choi, J. H., Ahn, J., Kim, J. B., Kim, Y. C., Lee, J. Y., & Oh, I. K. (2016). An Electroactive, Tunable, and Frequency Selective Surface Utilizing Highly Stretchable Dielectric Elastomer Actuators. *Small*.

[81] Benslimane, M., Gravesen, P., & Sommer-Larsen, P. (2002, July). Mechanical properties of dielectric elastomer actuators with smart metallic compliant electrodes. In *SPIE's 9th Annual International Symposium on Smart Structures and Materials* (pp. 150-157). International Society for Optics and Photonics.

[82] Rosset, S., Niklaus, M., Dubois, P., Dadras, M., & Shea, H. R. (2007, April). Mechanical properties of electroactive polymer microactuators with ion-implanted electrodes. In *The 14th International Symposium on: Smart Structures and Materials & Nondestructive Evaluation and Health Monitoring*(pp. 652410-652410). International Society for Optics and Photonics.

[83] Yuan, W., Brochu, P., Ha, S. M., & Pei, Q. (2009). Dielectric oil coated single-walled carbon nanotube electrodes for stable, large-strain actuation with dielectric elastomers. *Sensors and Actuators A: Physical*, *155*(2), 278-284.

[84] Pelrine, R., Kornbluh, R., Pei, Q., & Joseph, J. (2000). High-speed electrically actuated elastomers with strain greater than 100%. *Science*,*287*(5454), 836-839.

[85] Pourazadi, S., Ahmadi, S., & Menon, C. (2014). Towards the development of active compression bandages using dielectric elastomer actuators. *Smart Materials and Structures*, *23*(6), 065007.

[86] Pourazadi, S., Ahmadi, S., & Menon, C. (2015). On the design of a DEA-based device to pot entially assist lower leg disorders: an analytical and FEM investigation accounting for nonlinearities of the leg and device deformations. *Biomedical engineering online*, *14*(1), 1.

[87] Plante, J. S., & Dubowsky, S. (2007). On the properties of dielectric elastomer actuators and their design implications. *Smart Materials and Structures*, *16*(2), S227.

[88] Dupont Technical guide Kevlar® Aramid Fiber. Retrieved from http://www.dupont.com/content/dam/dupont/products-and-services/fabrics-fibers-and-nonwovens/fibers/documents/DPT_Kevlar_Technical_Guide_Revised.pdf

[89] Carpi, F., Anderson, I., Bauer, S., Frediani, G., Gallone, G., Gei, M., ... & Kollosche, M. (2015). Standards for dielectric elastomer transducers. *Smart Materials and Structures*, *24*(10), 105025.

[90] Ogden, R. W. (1972, February). Large deformation isotropic elasticity-on the correlation of theory and experiment for incompressible rubberlike solids. In*Proceedings of the Royal*

Society of London A: Mathematical, Physical and Engineering Sciences (Vol. 326, No. 1567, pp. 565-584). The Royal Society.

[91] Gatti, D., Haus, H., Matysek, M., Frohnapfel, B., Tropea, C., & Schlaak, H. F. (2014). The dielectric breakdown limit of silicone dielectric elastomer actuators. *Applied Physics Letters*, *104*(5), 052905.

[92] Rigden, J. S., & Pippard, B. (1997). Macmillan encyclopedia of physics.*Physics Today*, *50*, 65.

[93] Phung, H., Nguyen, C. T., Nguyen, T. D., Lee, C., Kim, U., Lee, D., ... & Choi, H. R. (2015). Tactile display with rigid coupling based on soft actuator.*Meccanica*, *50*(11), 2825-2837.

[94] Palakodeti, R., & Kessler, M. R. (2006). Influence of frequency and prestrain on the mechanical efficiency of dielectric electroactive polymer actuators.*Materials Letters*, *60*(29), 3437-3440.

[95] Fox, J. W., & Goulbourne, N. C. (2008). On the dynamic electromechanical loading of dielectric elastomer membranes. *Journal of the Mechanics and Physics of Solids*, *56*(8), 2669-2686.

[96] Works, H. I., & Rules, S. Reed Switch Motor.

[97] Gurevich, V. (2016). *Electric relays: Principles and applications*. CRC Press.

[98] *Littelfuse reed switch selection guide.* Littlefuse. Retrieved from http://www.littelfuse.com/~/media/electronics/application_guides/littelfuse_hamlin_reed_switch_selection_guide.pdf.pdf

[99] Huang, L., Pittini, R., Zhang, Z., & Andersen, M. A. (2014, November). Design comparison of autonomous high voltage driving system for DEAP actuator. In *2014 International Power Electronics and Application Conference and Exposition* (pp. 1061-1066). IEEE.

[100] Araromi, O. A., Conn, A. T., Ling, C. S., Rossiter, J. M., Vaidyanathan, R., & Burgess, S. C. (2011). Spray deposited multilayered dielectric elastomer actuators. *Sensors and Actuators A: Physical*, *167*(2), 459-467.